Near–IR properties of 24 Globular Clusters in the Galactic bulge [1]

E. Valenti

ESO – European Southern Observatory, Alonso de Cordoba 3107, Casilla 19001,

santiago 19, Chile

INAF – Osservatorio Astronomico di Bologna, Via Ranzani 1, I–40127 Bologna, Italy

evalenti@eso.org

F. R. Ferraro

Bologna University, Via Ranzani 1, I–40127 Bologna, Italy

and

L. Origlia

INAF – Osservatorio Astronomico di Bologna, Via Ranzani 1, I–40127 Bologna, Italy

Received _____; accepted _____

ABSTRACT

We present near–IR Color–Magnitude Diagrams and physical parameters for a sample of 24 Galactic Globular Clusters toward the Bulge direction. In this paper we discuss the properties of twelve new clusters (out of 24) in addition to those previously studied and published by our group. The compilation includes measurements of the cluster reddening, distance, photometric metallicity, Horizontal Branch Red Clump, Red Giant Branch morphological (i.e. mean ridge lines) and evolutionary (i.e. bump and tip) features. The compilation is available in electronic form through the WorldWideWeb, and it will be updated regularly.

Subject headings: globular clusters: general — Galaxy: bulge — infrared: stars — stars: imaging — technique: photometric

1. Introduction

In the last decades Galactic Globular Clusters (GCs) have proven to be extremely important astrophysical laboratories for a wide range of problematics. Indeed, the study of their stellar populations address fundamental questions ranging from stellar structure, evolution and dynamics to Galaxy formation and the early epoch of the Universe. Containing some of the oldest stars known, they are *fossils* from the remote and violent epoch of Galaxy formation. They also serve as test particles for studying Galaxy dynamics and to test stellar dynamical models. Being the largest aggregates in which all post Main Sequence (MS) stars can be individually observed, they serve as fiducial templates for understanding the integrated light from distant, unresolved stellar systems. In this respect, the Bulge GCs provide ideal templates to explore the high metallicity regime and thus to study the stellar content of extra–galactic bulges and Ellipticals. However, the high and patchy extinction, which makes optical observations difficult to impossible along most Bulge lines of sight, coupled with the limited performances of the past generation of near–IR instrumentation, prevented accurate determinations of the Bulge GCs basic properties (as age, metallicity, distance, etc), as already existing since a long time in the case of the Halo clusters. The current generation of ground–based IR instrumentation with high spatial resolution and wide field coverage, and with the future availability of the James Webb Space Telescope will allow us to resolve the brightest giants in galaxies up to several Mpc away. Hence, a homogeneous compilation of the Bulge GCs properties to be used as empirical templates of metal–rich stellar populations, is thus strongly urgent. In this framework, our group started a long–term project devoted to fully characterize the stellar populations in the Bulge GC system, by using color–magnitude diagrams (CMDs) and luminosity functions

[1]Based on data taken at the ESO/NTT Telescope, within the observing programs: 73.D–0313, 75.D–0372 and 77.D–0757.

(LFs) in the near–IR (see Ferraro et al. (2000) – hereafter F00; Valenti et al. (2004); Valenti, Ferraro & Origlia (2004a) – hereafter VFO04a; Valenti, Ferraro & Origlia (2004b) – hereafter VFO04b; Valenti, Origlia & Ferraro (2005) – hereafter VOF05; Origlia et al. (2005) – hereafter O05). The collected photometric database has been used to perform a detailed description of the main morphological and evolutionary features of the Red–Giant Branch (RGB) sequence, by means of a set of photometric indices, which have been defined and widely described in F00, and calibrated as a function of the cluster metallicity in VFO04a and VFO04b.

In this paper we present the largest, homogeneous near–IR photometric database of Bulge GC ever obtained. For each clusters, the compilation includes: *i)* the photometric catalog; *ii)* the RGB mean ridge line,; *iii)* accurate reddening, distance, and metallicity determinations; *iv)* the luminosity of the main RGB evolutionary features (i.e. the bump and the tip); and *v)* the mean magnitude of the Horizontal–Branch Red Clump (HB–RC). Moreover, in order to be easily accessible by the community, the compilation would be also provided in electronic form.

The programme cluster sample is presented in § 2, while § 3 is devoted to the detailed description of the observations, data reduction, and derived CMDs of a sample of 12 Bulge clusters, recently observed, and presented here for the first time. § 4 describes the overall characteristics of the compilation and the measurement of the HB–RC and the RGB bump and tip.

2. The entire sample

The cluster sample presented in this study counts 24 GCs in the Bulge direction observed in the near–IR by our group in the last few years. The targets selection has

been performed by defining *Bulge GCs* all those located within $|b| \leq 10^{\circ}$ and $|l| \leq 20^{\circ}$, where l and b are the Galactic coordinates, and giving a highest priority to the metal–rich population. Note that this definition is mainly a working hypothesis and refers to the position of the clusters in the Bulge direction, only. However, there are a number of growing evidences, based on kinematics (Dinescu et al. 2003) and high–resolution chemical abundances (Origlia, Valenti & Rich 2005, and references therein), favoring a Bulge origin for the metal–rich GCs within 3 Kpc from the Galactic center. Fig. 1 shows the spatial distribution in Galactic coordinates of our sample (which counts 50% of the entire Bulge GC system), and the COBE/DIRBE 3.5μm inner Bulge outline (Weiland et al. 1994). The clusters discussed in this paper fall into three categories:

Sample A – Seven clusters (NGC6342, NGC6380, NGC6440, NGC6441, NGC6528, NGC6553, NGC6624) have been already published, and a detailed description of the observations, data reduction and analysis can be found in F00, VFO04a, and VFO04b. This sample have been used to perform a detailed analysis of the main RGB morphological and evolutionary features, leading to an empirical calibration of suitable near–IR photometric indices (i.e. RGB color, magnitude, slope, bump and tip) as a function of the cluster metallicity.

Sample B – Five clusters (NGC6304, NGC6569, NGC6637, NGC6638, and NGC6539) have been presented in VOF05 and O05, where a detailed description of the derived IR–CMDs and the analysis of the RGB properties can be found. For this sample we derived the clusters metallicity by using the calibration of VFO04a,b.

Sample C – Twelve clusters (NGC6256, NGC6266, NGC6273, NGC6293, NGC6316, NGC6255, NGC6388, NGC6401, NGC6642, Ter3, Ter5, Ter6) are presented and discussed here for the first time.

3. Properties of Sample C

For this sample, a detailed description of the observations, data reduction, CMDs and physical properties of each cluster is provided in the following sub–sections.

3.1. Observations and data reduction

J, H and K_s images of the clusters in *Sample C* were obtained during three observing runs on June 2004, July 2005, and June 2006 using the near–IR camera SofI, mounted at the ESO/NTT telescope. During the observing runs two set of data were secured:

(i) Standard resolution set. A series of images in the J, H and K_s bands have been obtained by using SofI in *Large Field mode*, characterized by a pixel size of 0.288" and a total field of view of 4.9'× 4.9'. On average, the images are the combination of 42, 72, and 99 exposures each one 3–sec long in the J, H and K_s passbands, respectively.

(ii) High resolution set. High resolution images of the inner region of each cluster were also secured using the SofI focal elongator, yielding a pixel size of 0.146" and a total field of view 2.49' × 2.49'. High resolution images are the average of 30 single exposures 1.2 sec–long. All the secured images are roughly centered on the cluster center.

Note that the region covered by our observations allows us to sample a significant fraction of the total cluster light (typically ∼80-95%) in all the programme clusters. During the 8 nights of observations the average seeing was always quite good (FWHM≈0.8" − 1"). Every image has been background–subtracted by using sky fields located several arcmin away from the cluster center, and flat–field corrected using halogen lamp exposures, acquired with the standard SofI calibration setup.

Standard crowded field photometry, including PSF modeling, was carried out on each

frame by using DAOPHOTII/ALLSTAR (Stetson 1994). For each cluster, two photometric catalogs (derived from high and standard resolution images), listing the instrumental J, H and K_s magnitudes, were obtained by cross-correlating the single-band catalogs. The standard and high resolution catalogs have been combined by means of a proper weighted average, weighting more the high resolution measurements in the innermost region of the cluster. In principle, this strategy allows to minimize the blending effects. The internal photometric accuracy has been estimated from the *rms* frame–to–frame scatter of multiple stars measurements. Over most of the RGB extension, the internal errors are quite low ($\sigma_J \sim \sigma_H \sim \sigma_K < 0.03$ mag), increasing up to $\sim$0.06 mag at $K_s \geq 16$.

The instrumental magnitudes were then converted into the 2MASS photometric system[2], and the star positions astrometrized onto 2MASS[3] as done for the clusters in *Samples A and B*.

Since for Terzan 6 only high resolution data were acquired, we also used J, H and K' images obtained with the IRAC–2 camera (mounted at the ESO/MPI 2.2m telescope), in order to cover a larger area ($\approx$ 4'×4'). The derived calibrated catalog has been then merged with that one obtained from the SofI observations. Note that, as already discussed in Valenti et al. (2004) the calibration of the K' IRAC–2 photometry onto the K_s SofI one requires negligible color term.

Figure 2 presents the derived IR CMDs of the global sample of 24 GCs. As shown in the figure, the photometric catalogs span the entire RGB extension, from the Tip to $\approx$2-5 magnitudes below the HB (depending on the cluster extinction).

---

[2] An overall uncertainty of $\pm$0.05 mag in the zero–point calibration in all three bands has been estimated.

[3] The astrometric procedure provided *rms* residuals of $\approx$0.2 arcsec in both R.A. and DEC.

3.2. Reddening, distance and metallicity

The main cluster properties such as reddening and distance have been derived by using a differential method based on the comparison of CMDs and LFs of clusters with similar HB morphology. However, this method allows to derive reliable estimates of reddening and distance only for intermediate–high metallicity clusters, whose CMD shows a red clumpy HB morphology. In fact, the location in magnitude of the HB–LF peak can be used as a reference feature and safely compared with that one of the template cluster. In 5 metal–poor clusters (i.e. NGC6256, NGC6273, NGC6293, NGC6355 and NGC6401) the blue HB morphology coupled with the relatively high reddening and the remarkable level of field contamination prevented a safe location of the HB level, and thus the use of the differential method. Hence, in these cases the cluster reddening and distance have been obtained by using the empirical method presented by Ferraro, Valenti & Origlia (2006, – hereafter FVO06), which allows one to simultaneously get reddening, distance and metallicity of a stellar system by using a few observables, like the RGB slope, tip, and mean ridge line, of the [K, J–K] CMD.

The derived cluster reddening and distance have been used to transform the observed CMDs and RGB ridge lines into the absolute plane, and to measure the following parameters: *i)* $(J–K)_0$ and $(J–H)_0$ colors at 4 fixed absolute magnitude levels ($M_K = M_H = -5.5, -5, -4, -3$); *ii)* the absolute M_K and M_H magnitudes at constant $(J–K)_0 = (J–H)_0 = 0.7$ colors; and *iii)* the slope in the [K, J–K] and [H, J–H] planes. Then, by using the empirical calibrations from VFO04a linking this set of photometric indices to the cluster metal content, we finally derived the photometric metallicity estimates in the Carretta & Gratton (1997) scale. Hence, hereafter the notation [Fe/H] refers to the Carretta & Gratton (1997) scale. Note that, to derive the global metallicity [M/H], which takes into account the iron as well as the α–element abundances, we

used the calibrations presented in FVO06 within the Bulge-like enrichment scenario. Hence, accordingly to Carney's (1996) suggestions and the more recent results on the bulge populations (Origlia, Rich & Castro (2002); Origlia & Rich (2004); Zoccali et al. (2004); Origlia, Valenti & Rich (2005); Origlia et al. (2005); Carretta et al. (2006) for bulge clusters; and Rich & Origlia (2005); Cunha & Smith (2006); Zoccali et al. (2006); Fulbright, McWilliam & Rich (2006) for giant field stars) we adopted a [α/Fe]=0.30 constant over the entire range of metallicity up to solar [Fe/H].

In the next paragraphs we present the CMDs and RGB fiducial ridge lines for the 12 Bulge clusters of *Sample C*. We briefly discuss the main CMD properties, and we provide some references for previous published photometries.

NGC 6256

NGC 6256 is a heavily reddened cluster in the outer Bulge region. Its extinction, whose estimates range from E(B–V)=0.84 (Harris 1996, hereafter H96) to E(B–V)=1.66 (Schlegel et al. 1998, hereafter S98), prevented detailed photometric studies in the optical. Only two studies of the cluster can be found in the literature. The first by Barbuy et al. (1998) based on VI ground–based photometry, and the second by Piotto et al. (2002) based on HST BV observations. However, the derived CMDs show an extremely scattered RGB which is barely defined.

In our IR-CMD, shown in Fig. 2, the cluster RGB is rather scattered, suggesting the presence of a red component which might be due to the contamination by Bulge field stars. The HB appears as a blue vertical structure at (J–K)$\sim$0.5 and K$\leq$14 typical of low–intermediate metallicity. The almost blue vertical sequence, at 11.5$\leq$K$\leq$15 and 0.4$\leq$(J–K)$\leq$1, is likely due to the foreground disk stars. In order to investigate the nature

of the observed RGB spread, we compared the sequence morphology in the CMDs at different distances from the cluster center (see Fig. 3). As shown in Fig. 3, the reddest RGB component becomes progressively populated as the distance to the cluster center increases, thus confirming that it is due to field stars. As previously done for other highly contaminated clusters (see i.e. NGC 6304 in VOF05), the RGB fiducial ridge line has been derived considering only the innermost region of the cluster, typically only the stars lying within 30" from the cluster center. Since the absence of a prominent feature such as the red clumpy HB makes difficult to derive the cluster reddening and distance, we used the empirical method (see FVO06) rather than the differential one. From the analysis of the cluster CMD we estimated the RGB slope and the observed RGB-Tip to be RGB_{slope}=–0.052 and K^{Tip}=9.21, respectively. Using these values as input parameters, the computational routine (assuming the *Bulge–like scenario*), gives a reddening E(B–V)=1.2, an intrinsic distance modulus $(m\text{-}M)_0$=14.79, and metallicities [Fe/H]=–1.63 dex, and [M/H]=–1.43 dex. The distance estimate agree with the value by H96, and the derived metallicity is consistent with those published by Stephens & Frogel (2004) ([Fe/H]=–1.35 dex), based on low–medium resolution K spectra, and by Bica et al. (1998) ([Fe/H]=–1.01 dex) from integrated optical spectroscopy.

NGC 6266

NGC 6266 is a high density ($\log\rho$ ∼5.34, Djorgovski (1993)), moderately reddened (E(B–V)=0.44, H96; E(B–V)=0.47, S98) and massive (M_V=-9.19, H96) cluster, which has been subject of several dynamics, kinematics and stellar variability studies. In fact, this cluster turns out to be particularly interesting because: *i)* it is the fifth (after Ter 5, 47 Tuc, M 15 and M 28) ranking GC for wealth Millisecond Pulsars (MSPs), and it is the only GC exclusively populated by MSPs in binary systems (Possenti et al. 2003); *ii)* it hosts more

than 200 RR Lyrae variables (Contreras et al. 2005), whose periods place this cluster in the Oosterhoff type I group, though the cluster HB morphology (a blue HB component and a very extended blue tail) is similar to Oosterhoff type II GCs; *iii)* recent *Chandra* X–ray observations have revealed a very large number of X–ray sources, suggesting the presence of a high number of cataclysmic (and/or interacting) binaries; *iv)* its radial velocity is smaller than the escape velocity from the Bulge, indicating that, whatever its origin would be, it will never escape from the Bulge (Dinescu et al. 2003). Beccari et al. (2006) published the most extensive photometry based on a combination of multi–band high–resolution HST and wide–field ground based observations aimed at studying the cluster dynamical state, finding that the cluster has not experienced core collapse yet. No IR photometric studies for this cluster have been published so far.

The observed CMD in the [K, J–K] plane (see Fig. 2) shows a well populated RGB and a blue extended HB, suggesting a low–intermediate metallicity. As expected, in the near–IR plane the high level of contamination by foreground disk stars affecting the optical ground–based CMD of Beccari et al. (2006) is drastically reduced, allowing us a clear definition of the RGB ridge line from the tip down to the Sub–Giant Branch (SGB), at K$\sim$16. To estimate the cluster metallicity, we have adopted the distance modulus $(m–M)_0$=14.11 of Beccari et al. (2006) (based on the Ferraro et al. (1999, –hereafter F99) distance scale), and the reddening value from H96. The global set of photometric indices (in both [K, J–K] and [H, J–H] planes) computed for NGC 6266 have yielded a [Fe/H]=–0.98 dex and [M/H]=–0.82 dex, in good agreement with the values in the literature (see i.e. H96).

NGC 6273

NGC 6273 is an intermediate–low metallicity ([Fe/H]=–1.68, see H96), medium–concentration (c=1.5 Djorgovski 1993) cluster, and it is also the second most luminous (M_V=-9.50) in the Djorgovski (1993) compilation. It has been the subject of a monographic study by Piotto et al. (1999), based on HST B, V observations, aimed at understanding the nature of its extended HB blue tail, which shows a clear double–peaked distribution and a well defined gap. From the analysis of the CMD the authors estimated an intrinsic distance modulus $(m–M)_0$=14.77, and an average reddening E(B–V)=0.47, though their optical CMD is strongly affected by differential reddening (ΔE(B–V)=0.2 mag). The only IR CMD available in the literature is the one published by Davidge (2000), but it is poorly populated and quite shallow, reaching only K$\sim$15. From the [K, J–K] CMD, Davidge (2000) estimated a reddening E(B–V)=0.38, in excellent agreement with the value listed in literature (i.e. E(B–V)=0.38, H96, and E(B–V)=0.31, S98).

Fig. 2 shows our observed CMD in the [K, J–K] plane along with the derived RGB ridge line (solid line). The cluster RGB is well populated even in the brightest magnitude bin, and the HB appears as a vertical structure almost parallel to the RGB at (J–K)$\sim$0.2, suggesting a low–intermediate metallicity. Our photometry is deep enough to reach $\sim$1 mag below the Main Sequence–Turn Off (MS–TO), however the SGB is quite scattered, preventing an accurate measurement of the MS–TO luminosity, hence a reliably cluster age estimate. Because of its HB morphology, the cluster reddening and distance have been derived by using the empirical method of FVO06. From the analysis of the observed CMD we derived the RGB slope (RGB_{slope}=–0.063) and the the RGB tip (K^{Tip}=8.57). Adopting these two values as input parameters, we found E(B–V)=0.40, $(m–M)_0$=14.58, [Fe/H]=–1.40, and [M/H]=–1.21, for the cluster reddening, distance and metallicity, respectively. The derived distance is consistent (within 0.2 mag) with the Piotto et al. (1999) estimate and (within

0.1 mag) with the value listed by H96. Our reddening measurement agree well with the values in literature (see i.e. H96, S98, Piotto et al. (1999); Davidge (2000)).

NGC 6293

NGC 6293 is the most metal–poor cluster in the observed sample. In the literature, the best available photometries are those published by Davidge (2000) and Piotto et al. (2002). Piotto et al. (2002) presented HST B, V CMD, which shows an extended blue HB, confirming the low metal content of this cluster. The near–IR CMD of Davidge (2000) is poorly populated, and only reaches K$\sim$15. From the IR data, the author estimated a reddening E(B–V)=0.04, which is significantly lower than the value listed in the literature (E(B–V)= 0.39, H96; E(B–V)= 0.60, S98). A careful examination of the derived CMD in Fig. 2, reveals the presence of a quite scattered RGB, which cannot be explained in terms of photometric errors. In order to understand the nature of the observed scatter, as already done for NGC 6256, in Fig. 4 we compared the radial CMDs in 4 annuli at different distances from the cluster center. In the innermost 30" region (Fig. 4, *panel a*) the RGB is quite narrow, and progressively spread out with increasing the distance from the cluster center. A field component redder than the cluster RGB is present at r>60". This high level of field contamination is not surprising since NGC 6293 lies in the Ophiuchus complex, a dense stellar region towards the Galactic center. Hence, the RGB fiducial ridge line has been derived using only the stars in the innermost 30" cluster region, where the field contamination is low. The measured reddening, distance, and metallicity estimates (E(B–V)=0.30, $(m–M)_0$=15.10, [Fe/H]=–1.73, and [M/H]=–1.55) have been obtained by using the empirical method of FVO06, with the following input parameters: RGB_{slope}=–0.048 and K^{Tip}=9.24. The derived cluster parameters nicely agree with the corresponding values listed by H96. In particular, the derived photometric metallicity is

consistent (within ≈0.2 dex) with the spectroscopic estimate published by Lee & Carney (2002) (i.e. [Fe/H]=–1.99 dex).

NGC 6316

Among the observed clusters, NGC 6316 is one of the most metal–rich and with the largest distance to the Galactic center. The [K, V–K] CMD presented by Davidge et al. (1992) shows a red clumpy HB and a quite well populated upper RGB, the photometry reaching only ∼1 mag below the HB. They estimated a reddening E(B–V)=0.6, which is consistent within the values listed by H96 (E(B–V)=0.55) and byS98 (E(B–V)=0.98). Piotto et al. (2002) presented a HST [V, B–V] CMD of this cluster, showing a HB morphology close to that of 47 Tuc. However the moderately high reddening, and the contamination by foreground disk stars prevented a clear definition of the RGB, which appears considerably scattered even in the brightest bins. As shown in Fig. 2 our CMD in the [H, J–H] plane is deep enough to properly sample the entire RGB, from the base up to the tip, thus allowing us a safe definition of the RGB fiducial ridge line. From the CMD and the derived LF, we estimated a reddening E(B–V)=0.56, which is intermediate between the Davidge et al. (1992) and H96 estimates, and an intrinsic distance modulus $(m–M)_0$=15.33, slightly longer (∼0.13 mag) than the H96 value. Since no K–band data were taken for this cluster, to estimate its metallicity we only measured the photometric indices in the [H, J–H] plane. Our findings, [Fe/H]=–0.60 dex and [M/H]=–0.45 dex, nicely agree with the value listed by H96, confirming that NGC 6316 has a metallicity slightly higher than 47 Tuc, as previously suggested by Davidge et al. (1992) on the basis of the RGB slope measurement.

NGC 6355

NGC 6355 lies behind a dark nebula in the eastern extension of the Ophiuchus complex, and it is thus affected by a relatively high extinction (i.e. E(B–V)=0.75, H96; E(B–V)=1.15, S98). Ortolani et al. (2003) published a [V, V–I] CMD showing a large field contamination and a barely detectable blue HB. From the analysis of the CMD, the authors found E(B–V)=0.78, $(m–M)_0$=14.73 and [Fe/H]=–1.3 dex.

Our derived CMD, shown in Fig. 2, exhibits a blue HB at $0.2 \leq (J–K) \leq 0.6$ and $14.5 \leq K \leq 16$, and a quite scattered RGB. As expected, in the [K, J–K] and [H, J–H] planes, the high level of contamination by disk stars strongly affecting the Ortolani et al. (2003) CMD, is significantly reduced. However, in our CMD the main source of contamination is due to the foreground Bulge field stars, which produce the observed RGB split. In fact, as shown in the radial CMDs of Fig. 5, by increasing the distance from the cluster center, a secondary red component becomes progressively more pronounced, causing the observed scatter in the RGB. As done for NGC 6256 and NGC 6293, the RGB ridge line has been derived by using only the stars lying within 30" from the cluster center, and the main cluster properties have been estimated by using the empirical method of FVO06. From the observed CMDs, we measured RGB_{slope}=–0.068 and K_{Tip}=8.854. Adopting these two values we find E(B-V)=0.82, $(m-M)_0$=14.70, [Fe/H]=–1.42 dex and [M/H]=–1.22 dex for the cluster reddening, distance and metallicity. Our findings nicely agree with the Ortolani et al. (2003) results.

NGC 6388

NGC 6388 is a moderately reddened (i.e. E(B–V)=0.37, H96; E(B–V)=0.39, S98; E(B–V)=0.40, Pritzl et al. (2002)), metal–rich ([Fe/H]=-0.60, H96, Pritzl et al. (2005))

cluster located in the outer Bulge region (see Fig. 1). Since the discovery by Rich et al. (1997) of an extended blue HB (as well as in NGC 6441) in its HST–based CMD, NGC 6388 has been subject of several optical photometric studies (see i.e. Moehler, Sweigart & Catelan 1999; Piotto et al. 2002; Pritzl et al. 2002, and reference therein). NGC 6388 displays a quite peculiar HB morphology. In fact, besides a well populated red HB clump (a feature normally predicted by the stellar evolution theory in the case of old, metal–rich populations) it shows an extended blue tail and a population of RR Lyrae variables (Pritzl et al. 2002). NGC 6388 and NGC 6441 are thus the most metal–rich examples of *Second–parameter* affecting the HB morphology. From the analysis of the cluster CMD based on Washington photometry, Hughes et al. (2006) claimed that NGC 6388 has a RGB too broad to be chemically homogeneous, suggesting a metallicity spread of δ[Fe/H]=$\sim$0.3 dex. However, very recently, no intrinsic metallicity spread has been found by Carretta et al. (2006), who performed high–resolution (R$\approx$40,000) optical spectroscopy of seven cluster members, finding an average [Fe/H]=–0.44 dex with a *rms*=0.04 dex.

No IR photometric studies have been published so far for this cluster. Fig. 2 shows the first CMD in the [K, J–K] plane, and the derived RGB ridge line. As expected, the observed CMD is characterized by a well defined red HB clump suggesting a high metallicity, while the extended blue HB is barely visible as the vertical structure at 15.5$\lesssim$K$\lesssim$17.5 and 0$\lesssim$(J–K)$\lesssim$0.6. The RGB appears well populated over its entire extension, from the base (K$\sim$17) up to the tip, allowing us a detailed description of its morphological features. From the comparison of the cluster CMDs and LFs with those of 47 Tuc, we estimated the reddening and distance to be E(B–V)=0.44 and $(m–M)_0$=15.38, respectively. The photometric indices measured along the RGB, in the [M_K, $(J–K)_0$] and [M_H, $(J–H)_0$] absolute planes, yielded the following metallicity estimates: [Fe/H]=–0.61 dex and [M/H]=–0.42 dex, in good agreement with previous literature values.

NGC 6401

NGC 6401 is located in the inner Bulge region, at ∼0.8 Kpc (see Table 1 and Fig. 1) from the Galactic center. Its physical parameters are not well determined in the literature. In particular, the extinction estimates range from E(B–V)=0.53 (Barbuy et al. 1999) to E(B–V)=0.98 (S98), and the cluster distance values are between $(m–M)_0$=14.39 (H96) and $(m–M)_0$=14.76 (Barbuy et al. 1999). From the analysis of the observed [V, V–I] CMD, Barbuy et al. (1999) concluded that NGC 6401 is metal–rich, with a metallicity close to 47 Tuc, while from low–resolution optical spectroscopy Minniti (1995) found [Fe/H]=–1.1 dex.

The near–IR CMD here obtained is shown in Fig. 2, along with the derived RGB ridge line. The most interesting features are: *i)* a blue HB tail at 0.4≤(J–K)≤0.9 and 13≤K≤16; *ii)* a rather scattered RGB, which seems split in 2 separated sequences, particularly in the [K, J–K] plane. Note that, the presence of a blue extended HB is confirmed by the Piotto et al. (2002) work based on HST BV observations.

Fig. 6 clearly shows that, in the innermost region, within 30" from the cluster center, the CMD exhibits a blue HB and a quite narrow RGB, while by increasing the distance from the cluster center the CMD starts to be characterized by a red clumpy HB and by a RGB significantly redder than the cluster mean loci. Hence, the observed RGB spread is likely due to the bulk of the Bulge field population which is metal–rich. In order to derive the cluster main properties we used the FVO06 empirical method, assuming the *Bulge–like scenario*. We measured the cluster RGB slope considering only those stars lying in the innermost cluster region (RGB_{slope}=-0.065) and we estimated the observed (K=8.69) RGB tip by using the brightest stars in our catalog lying along the RGB ridge line. We used these values as input parameters for the computational routine and we obtained the following reddening, distance and metallicity estimates: E(B–V)=1.1, $(m–M)_0$=14.43,

[Fe/H]=–1.37 dex and [M/H]=–1.20 dex. The derived photometric metallicity is consistent with the spectroscopic result by Minniti (1995) (Δ[Fe/H]=0.25 dex) and significantly lower than that found by Barbuy et al. (1999) (Δ[Fe/H]$\sim$0.7 dex).

NGC 6642

The moderately reddened cluster NGC 6642 (i.e. E(B–V)=0.41, H96; E(B–V)=0.40, S98) has been observed in the IR and in the optical by Davidge (2000) and Piotto et al. (2002), respectively. However both the published CMDs show sequences which are not well populated, and with a remarkable scatter. Fig. 2 shows our derived CMD in the [H, J–H] plane, along with the mean RGB ridge line. The main features of the CMD are a blue HB and a steep RGB, typical of low–intermediate metallicity clusters. In this case, since no K photometry is available, the reddening and the distance have been estimated by matching the cluster sequence loci in the CMD to those of the reference cluster NGC 6752. By using our derived reddening (E(B–V)=0.60) and distance ((m–M)$_0$=14.68), we measured the photometric indices, giving the following photometric metallicity estimates: [Fe/H]=–1.20 dex and [M/H]=–1.03 dex. These values are fully consistent (within 0.2 dex) with the corresponding values listed by H96 ([Fe/H]=–1.35) and by Minniti (1995) ([Fe/H]=–1.40), based on low–resolution optical spectroscopy. Note that, also the obtained distance nicely agree with the value listed by H96 (i.e. (m–M)$_0$=14.63).

Terzan 3

Terzan 3 is a low concentration cluster (c=0.70, Djorgovski (1993)) projected on the outskirts of the Bulge (see Fig. 1). The only published photometry is the one by Barbuy et al. (1998). From the analysis of the derived [V, B–V] CMD, whose major features

are a red HB and a moderately bent RGB, they derived E(B–V)=0.72, $(m–M)_0$=14.05 and [Fe/H]∼–0.70 dex.

Our CMD along with the RGB fiducial ridge line is shown in Fig. 2. This high–resolution IR photometry reaches ∼2 mag below the MS–TO. The presence of a red clumpy HB at K∼13.42 suggests a moderately high metallicity, like 47 Tuc. The analysis of the cluster CMDs and LFs yields a reddening E(B–V)=0.73 (in excellent agreement with the values found by Barbuy et al. (1998) and S98), an intrinsic distance modulus $(m–M)_0$=14.54 and metallicities [Fe/H]=–0.82 dex and [M/H]=–0.63 dex. The significant (∼0.5 mag) discrepancy between our and Barbuy et al. (1998) distance is due to a different assumption for the selective–to–total absorption coefficient (R_V=3.1, in this study; R_V=3.3 in the Barbuy et al. (1998) work) and for the distance scale (F99 here, and Jones et al. (1992) in Barbuy et al. (1998) paper).

Terzan 5

Terzan 5 is a compact and massive cluster located in the very inner Bulge region. In the last few years this extremely dense cluster has been subject of several studies aimed at investigating its stellar population (i.e. Ortolani et al. 1996, 2001; Cohn et al. 2002; Origlia & Rich 2004), as well as at understanding stellar interactions and GC dynamics (i.e. Heinke et al. 2003; Ransom et al. 2005), having the highest stellar interaction rate of any Galactic GC (Verbunt & Hut 1987). In fact among GCs, Ter 5 ranks first in wealth of MSPs, and it hosts many interacting binaries (i.e. cataclysmic variables, X–ray binaries). Being embedded in a heavily obscured zone, it is affected by a large differential reddening which makes optical observations almost impossible. In fact, the only available optical photometry is that by Ortolani et al. (1996) who published a CMD in the [I, V–I] plane, showing largely scattered RGB and HB. They estimated E(B–V)=2.49, $(m–M)_0$=13.74 and

a metallicity close to NGC 6553 (i.e. [Fe/H]=–0.3, (Origlia, Rich & Castro 2002)). Later on, a [J, J–H] CMD based on HST observations has been published by Ortolani et al. (2001) and Cohn et al. (2002) with the aim of deriving more accurate cluster parameters such as reddening, distance, and age. From the analysis of the derived CMD, Ortolani et al. (2001) found Ter 5 to be coeval to NGC 6528. Cohn et al. (2002) obtained an IR–CMD significantly deeper (∼2mag), confirming the age found by Ortolani et al. (2001). They, also derived E(B–V)=2.16 and $d_{\odot}$=8.7 Kpc.

Fig. 2 shows our observed CMD in the [K, J–K] plane along with the derived RGB ridge line. The dominant features of the IR–CMD are: *i)* a red clumpy HB; and *ii)* a well populated RGB, from the base (K∼16) up to the tip (K∼8.5), which allow us a clear definition of its ridge line. From the analysis of the CMD and LF we derived E(B–V)=2.38, and $(m–M)_0$=13.87. The reddening value is in between the estimates provided by Ortolani et al. (1996) and Cohn et al. (2002), while our distance measurement is fully consistent with the one of Ortolani et al. (1996). The photometric indices measured along the cluster RGB by adopting the reddening and distance quoted above, lead the following metallicity estimates: [Fe/H]=–0.32 dex and [M/H]=–0.19 dex, thus in excellent agreement with the high–resolution IR spectroscopic result obtained by Origlia & Rich (2004) ([Fe/H]=–0.21 dex).

Terzan 6

Terzan 6 is another example of heavily reddened cluster in the inner Bulge region. The only available photometric study is the one by Barbuy et al. (1997), which provided a [I, V–I] CMD. The authors estimated the cluster reddening (E(B–V)=2.24) by comparing the derived CMD with that of NGC 6553, the cluster distance ($(m–M)_0$=14.23) by using the absolute V magnitude of the HB level, and from the RGB morphology they concluded that

Ter 6 shows intermediate characteristics between 47 Tuc and NGC6528/NGC6553.

Our IR observations of Ter 6 provided the first IR–CMD (see Fig. 2) showing a red HB and a curved RGB which are both high–metallicity indicators. From the derived CMD we found E(B–V)=2.35 and $(m–M)_0$=14.13. Both estimates nicely agree with the corresponding values found by Barbuy et al. (1997). The set of IR photometric indices measured by using the RGB ridge lines give a cluster metallicity of [Fe/H]=–0.62 dex and [M/H]=–0.43 dex.

4. The final Compilation

The compilation presented in this study is publicy available through the World-WideWeb. The Website address is:

http://www.bo.astro.it/∼GC/ir_archive

For the entire cluster sample, two separate files are available: the first list the J, H and K photometry for all the measured stars in each cluster, together with the stars absolute position in R.A. and Dec.; the second reports the observed RGB fiducial ridge line in the [K, J–K] and [H, J–H] planes.

Table 1 lists the derived parameters for the 24 clusters, namely the reddening, the distance and the metallicity in both the adopted scales (columns [9,10,11,12], respectively). Moreover, by using our distance determinations, the *(l, b)* Galactic coordinates from H96, and assuming a distance R_0=8 Kpc to the Galactic center (Eisenhauer et al. 2003), we also provided new estimates of the clusters distance from the sun ($d_\odot$), from the Galactic center (R_{GC}), and the distance components X, Y, Z, in a Sun–centered coordinate system (columns

[4,5,6,7,8], respectively). Finally for each cluster, column [13] lists the references for the IR photometry. It is worth mentioning that Table 1 lists the largest, homogeneous compilation of Bulge GCs obtained so far, whose properties have been derived in a self–consistent way. In fact, the derived cluster reddening, distance and metallicity are based on *i)* a homogeneous photometric database analyzed by using the same data reduction procedures, and calibrated onto the 2MASS photometric system; *ii)* the F99 distance scale; *iii)* a uniform and high–resolution metallicity scale (Carretta & Gratton 1997).

A summary table with the derived parameters for the global sample of clusters, here split in Tables 1 and 2, is also provided in a easily machine–readable format.

4.1. The RGB Bump and Tip

The most interesting evolutionary features along the RGB are the so–called bump and tip. The former flags the point (during the post–MS evolution of low mass stars) when the narrow hydrogen–burning shell reaches the discontinuity in the hydrogen distribution profile, generated by the previous innermost penetration of the convective envelope. Besides providing an obvious check on the accuracy of theoretical models of stellar evolution, the identification of the RGB bump in stellar systems can be used as useful tool for providing observational constraints on a number of population parameters, since it is a sensitive function of metal content, helium abundance and stellar population age. From the observational point of view, as emphasized by Fusi Pecci et al. (1990) and F99, the combined use of the differential and integrated LFs is the best tool to properly detect the bump.

The evolution along the RGB ends at the so–called RGB tip with helium ignition in the stellar core. In GC stars, this event is moderately violent because it takes place in a

electron–degenerate core. Because the RGB reaches its maximum extension in luminosity for stellar populations older than $\tau \approx$1–2 Gyr (i.e. when stars with M$\leq$ 2.0M$_\odot$ are evolving off the MS) and it remains approximately constant with increasing the age of the population, the tip is now widely used as a standard candle for distance determination of stellar systems.

The dependence of the RGB bump and tip luminosities (in the J, H and K bands. as well as in bolometric) on the cluster metallicity has been investigated in VFO04b. Here we have extended the same study to the new sample of Bulge clusters. In doing this, we have adopted the same strategy followed in that paper, where the reader can find a detailed description of the adopted procedures.

For the entire sample, the measurements of the main evolutionary features are listed in Table 2: the observed J, H, and K magnitude of the red HB clump (columns [4, 5, 6]), the J, H, K and bolometric bump (columns [7, 8, 9, 13], respectively), and tip (columns [10, 11, 12, 14], respectively) magnitudes. The bolometric bump and tip magnitude have been obtained by using the bolometric corrections for Population II giants computed by Montegriffo et al. (1998).

Fig. 7 shows the absolute RGB tip magnitudes as a function of the metallicity, in both the adopted scales. The clusters tip determination nicely agree with the empirical relations by VFO04b (solid lines), and with the theoretical prediction by Straniero, Chieffi & Limongi (1997); Cassisi et al. (2000) (dashed and dotted line, respectively). As shown in Fig. 8, a good agreement is also found when we compare the bolometric tip magnitudes, as a function of the clusters metallicity, with the VFO04b empirical relation (solid lines), and with four different theoretical expectations by Caloi et al. (1997); Salaris & Cassisi (1997); Girardi et al. (2000) (dashed, dotted and dotted–dashed lines, respectively).

Fig. 9 plots the absolute J, H and K bump magnitudes of the bulge (filled circles) and

Halo (open circles) clusters (the latter presented in VFO04b) *vs* metallicity, showing that the bump becomes rapidly fainter by increasing the latter. Hence, since with the present study we both enlarged the sample of high metallicity clusters and adopted the recent [Fe/H] estimates by Origlia, Rich & Castro (2002); Origlia, Valenti & Rich (2005) based on high–resolution IR spectroscopy, for the two most metal–rich objects in our sample (namely, NGC 6528 and NGC 6553), we calibrated new relations. As shown in Fig. 9 the new calibrations (solid lines) differ from the VFO04b ones (dashed lines) only in the metal–rich tail, making the bump somewhat brighter. The new calibrations of the bump J, H, K absolute magnitude, in both the adopted metallicity scales, are as follows:

$$M_J^{Bump} = 0.39 + 1.63[Fe/H] + 0.28[Fe/H]^2 \quad (1)$$

$$M_H^{Bump} = -0.12 + 1.68[Fe/H] + 0.34[Fe/H]^2 \quad (2)$$

$$M_K^{Bump} = -0.25 + 1.57[Fe/H] + 0.27[Fe/H]^2 \quad (3)$$

$$M_J^{Bump} = 0.10 + 1.53[M/H] + 0.28[M/H]^2 \quad (4)$$

$$M_H^{Bump} = -0.37 + 1.65[M/H] + 0.38[M/H]^2 \quad (5)$$

$$M_K^{Bump} = -0.53 + 1.47[M/H] + 0.27[M/H]^2 \quad (6)$$

Fig. 10 shows the bolometric magnitude of the bump as a function of the cluster metallicity, together with the new best–fit relations:

$$M_{Bol}^{Bump} = 1.93 + 1.73[Fe/H] + 0.29[Fe/H]^2 \quad (7)$$

$$M_{Bol}^{Bump} = 1.62 + 1.61[M/H] + 0.28[M/H]^2 \quad (8)$$

The comparison between the data and the theoretical models by Straniero, Chieffi & Limongi (1997); Girardi et al. (2000); Pietrinferni et al. (2004) (see lower panel of Fig. 10) shows an overall good agreement.

Part of the data analysis has been performed with the software developed by P. Montegriffo at the Osservatorio Astronomico di Bologna (INAF–AOB).

The MIUR (Ministero dell'Istruzione, dell'Universitá e della Ricerca) is kindly acknowledged for the financial support.

We warmly thanks the ESO-La Silla Observatory Staff for assistance during the observations.

This publication makes use of data products from the Two Micron All Sky Survey, which is a joint project of the University of Massachusetts and Infrared Processing and Analysis Center/California Institute of Technology, founded by the National Aeronautics and Space Administration and the National Science Foundation.

REFERENCES

Barbuy, B., Ortolani, S. & Bica, E. 1997, A&AS, 122, 483

Barbuy, B., Bica, E. & Ortolani, S. 1998, A&AS, 333, 117

Barbuy, B., Ortolani, S. &Bica, E. 1998, A&AS, 132, 33

Barbuy, B., Ortolani, S., Bica, E., Desidera, S. 1999, A&A, 348, 783

Beccari, G., Ferraro, F. R., Possenti, A., Valenti, E., Origlia, L., Rood, R. T. 2006, AJ, 131, 2551

Bica, E., Clariaa, J. J., Piatti, A. E., Bonatto, C. 1998, A&AS, 131, 483

Caloi, V., D'Antona, F. & Mazzitelli, I. 1997, A&A, 320, 823

Carretta, E. & Gratton, R. G. 1997,A&AS, 121, 95

Carretta, E., Bragaglia, A., Gratton, R. G., Momany, Y., Recio–Blanco, A. et al. 2006, A&A, submitted

Cassisi, S., Castellani, V., Ciarcelluti, P., Piotto, G., Zoccali, M. 2000, MNRAS,

Cohn, H.N., Lugger, P. H., Grindlay, J. E. & Edmonds, P. D. 2002, AJ, 571, 818

Contreras,R., Catelan, M., Smith, H. A.; Pritzl, B. J.; Borissova, J. 2005, ApJ, 623, L117

Cunha, K. & Smith, V. V. 2006, ApJ, astro–ph/0607393

Davidge, T. J., Harris, W.E., Bridges, T. J., Hanes, D.A. 1992, ApJS, 81, 251 315, 679

Davidge, T. J. 2000, AJ, 120, 1875

Dinescu, D. I., Girard, T. M., Van Altena, W. F., Lopez, C. E. 2003, AJ, 125, 1373

Djorgovski, S. 1993, in ASP Conf. Ser. 50, *Structure and Dynamics of Globular Clusters*, eds. S. Djorgovski & G. Meylan

Eisenhauer, F., Schodel, R., Genzel, R., Ott, T., Tecza, M., Abuter, R., Eckart, A., Alexander, T., 2003, ApJ, 597, L121

Ferraro, F. R., Messineo, M., Fusi Pecci, F., De Paolo, M. A., Straniero, O., Chieffi, A., Limongi, M. 1999, AJ, 118, 1738 (F99)

Ferraro, F. R., Montegriffo, P., Origlia, L., Fusi Pecci, F. 2000, AJ, 119, 1282 (F00)

Ferraro, F. R., Valenti, E. & Origlia, L. 2006, ApJ, 649, 243 (FVO06)

Fulbright, J. P., McWilliam, A., & Rich, M. R. 2006, astro-ph/0609087

Fusi Pecci, F., Ferraro, F. R., Crocker, D. A., Rodd, T. R. & Buonanno, R. 1990, A&A, 238,95

Girardi, L., Bressan, A., Bertelli, G. & Chiosi, C. 2000, A&AS, 141, 371

Harris, W. E. 1996, AJ, 112, 1487 (H96)(for the 2003 updated version see http://physwww.mcmaster.ca/%7Eharris/mwgc.dat)

Heinke, C. O., Edmonds, P. D., Grindlay, J. E., Lloyd, D. A., Cohn, H. N., Lugger, P. M. 2003, AJ, 590, 809

Hughes, J. D., Wallerstein, G., Covarrubias, R., Hays, N. 2006, AAS, 208, 6501

Jones, R. V., Carney, B. W., Storm, J., Latham, D. W, 1992, ApJ, 386, 646

Lee, J.-W. & Carney, B. W. 2002, AJ, 124, 1511

Minniti, D. 1995, A&A, 303, 468

Moehler, S., Sweigart, A. V. & Catelan, M. 1999, A&A, 351, 519

Montegriffo, P., Ferraro, F. R., Origlia, O.,Fusi Pecci, F. 1998, MNRAS, 297, 872

Origlia, L., Rich, R. M., & Castro, S. 2002, AJ, 123, 1559

Origlia, L., & Rich, R. M. 2004, AJ, 127, 3422

Origlia, L., Valenti, E., Rich, R. M., Ferraro, F. R. 2005, MNRAS, 363, 897 (O05)

Origlia, L., Valenti, E. & Rich, R. M. 2005, MNRAS, 356, 1276

Ortolani, S., Barbuy, B. & Bica, E. 1996, A&A, 308, 733

Ortolani, S., Barbuy, B., Bica, E., Renzini, A., Zoccali, M., Rich, R. M. & Cassisi, S. 2001, A&A, 376,878

Ortolani, S., Bica, E. & Barbuy, B. 2003, A&A, 402, 565

Pritzl, B. J., Smith, H. A., Catelan, M., Sweigart, A. V. 2002, AJ, 124, 949

Pritzl, B. J., Venn, K. A., Ivans, I. I., Catelan, M., Layden, A. C., Kinemuchi, K., Rich, R. M., Sweigart, A. V. 2005, AAS, 206, 3601

Pietrinferni, A., Cassisi, S., Salaris, M. & Castelli, F. 2004, ApJ, 612, 168

Piotto, G., Zoccali, M., King, I. R., Djorgovski, S. G., Sosin, D., Rich, R. M. & Meylan, G. 1999, AJ, 118,1727

Piotto, G., King, I. R., Djorgovski, S. G., Sosin, D., Zoccali, M., Saviane, I., De Angeli, F., Riello, M., Recio Blanco, A., Rich, R. M., Meylan, G. & Renzini, A. 2002 A&A, 391,945

Possenti, A., D'Amico, N., Manchester, R. N., Camilo, F., Lyne, A. G., Sarkissian, J. & Corongiu, A. 2003, ApJ, 599, 475

Rich, R. M. et al. 1997, ApJ, 484,25

Rich, R.M., & Origlia, L. 2005, ApJ,634, 1293

Schlegel, D. J., Finkbeiner, D. P., & Davis, M. 1998, ApJ, 500, 525 (S98)

Salaris, M. & Cassisi, S. 1997, MNRAS, 289, 406

Stephens, A. W. & Frogel, J. A. 2004, AJ, 127, 925

Stetson, P. B. 1987, PASP,99,191

Straniero, O., Chieffi, A. & Limongi, M. 1997, ApJ, 490,425

Ransom, S. M., Hessels, J. W., Stairs, I. H., Freire, P. C. C., Camilo, F., Kaspi, V. M., Kaplan, D. L. 2005, Science, 307, 892

Valenti, E., Ferraro, F. R., Perina, S., Origlia, L. 2004, A&A, 419, 139

Valenti, E., Ferraro, F. R. & Origlia, L. 2004, MNRAS, 351, 1204 (VFO04a)

Valenti, E., Ferraro, F. R. & Origlia, L. 2004, MNRAS, 354, 815 (VFO04b)

Valenti, E., Origlia, L. & Ferraro, F. R. 2005, MNRAS, 361, 272 (VOF05)

Verbunt, F. & Hut, P. 1987, IAU Symp. 125, The Origin and Evolution of Neutron Stars, ed. D. J. Helfand & H. H. Huang (Dordrecht:Reidel), 187

Weiland, J. L., Arendt, R. G., Berriman, G. B., Dwek, E., Freudenreich, H. T., et al. 1994, AJ, 425, L81

Zoccali, M., Barbuy, B., Hill, V., Ortolani, S., Renzini, A., Bica, E., Momany, Y., Pasquini, L., Minniti, D., Rich, R. M. 2004, A&A, 423, 507

Zoccali, M., Lecureur, A., Barbuy, B., Hill, V., Renzini, A., Minniti, D., Momany, Y., Gomez, A., Ortolani, S. 2006, A&A, 457L, 1

This manuscript was prepared with the AAS LaTeX macros v5.2.

Table 1. Coordinates, distance, reddening and metallicity for the global sample of Bulge clusters.

Name	l°	b°	$d_\odot$ (Kpc)	R_{GC} (Kpc)	X (Kpc)	Y (Kpc)	Z (Kpc)	E(B–V)	$(m–M)_0$	[Fe/H]	[M/H]	Ref.
6256*	-12.21	3.31	9.1	2.2	8.9	-1.9	0.5	1.20	14.79	-1.63	-1.43	tw
6266	-6.42	7.32	6.6	1.8	6.5	-0.7	0.8	0.47	14.11	-0.99	-0.80	tw
6273*	-3.13	9.38	8.2	1.4	8.1	-0.4	1.3	0.40	14.58	-1.40	-1.21	tw
6293*	-2.38	7.83	10.5	2.8	10.4	-0.4	1.3	0.30	15.10	-1.73	-1.55	tw
6304	-4.17	5.38	6.0	2.2	5.9	-0.4	0.6	0.58	13.88	-0.75	-0.56	VOF05
6316	-2.82	5.76	11.6	3.8	11.6	-0.6	1.2	0.56	15.33	-0.58	-0.38	tw
6342	4.90	9.73	8.4	1.6	8.3	0.7	1.4	0.57	14.63	-0.71	-0.53	VFO04a
6355*	-0.42	5.43	9.0	1.1	8.7	-0.1	0.8	0.81	14.77	-1.42	-1.22	tw
6380	-9.82	-3.42	9.2	1.9	9.0	-1.6	-0.5	1.29	14.81	-0.87	-0.68	VFO04a
6388	-14.44	-6.74	11.9	4.8	11.5	-3.0	-1.4	0.44	15.38	-0.61	-0.42	tw
6401*	3.45	3.98	7.7	0.8	7.7	0.5	0.5	1.10	14.43	-1.37	-1.20	tw
6440	7.73	3.80	8.2	1.2	8.1	1.1	0.5	1.15	14.58	-0.49	-0.40	VFO04a
6441	-6.47	-5.01	13.5	5.7	13.4	-1.5	-1.2	0.52	15.65	-0.68	-0.52	VFO04a
6528	1.14	-4.17	7.5	0.8	7.5	0.1	-0.5	0.62	14.37	-0.17	+0.04	F00
6539	20.80	6.78	8.4	3.1	7.8	3.0	1.0	1.08	14.63	-0.79	-0.60	O05
6553	5.25	-3.02	4.9	3.2	4.9	0.4	-0.3	0.84	13.46	-0.30	-0.09	F00
6569	0.48	-6.68	12.0	4.2	11.9	0.1	-1.4	0.49	15.40	-0.85	-0.66	VOF05
6624	2.79	-7.91	8.4	1.3	8.3	0.4	-1.2	0.28	14.63	-0.63	-0.48	VFO04a

Table 1—Continued

Name	l°	b°	$d_\odot$ (Kpc)	R_{GC} (Kpc)	X (Kpc)	Y (Kpc)	Z (Kpc)	E(B–V)	$(m–M)_0$	[Fe/H]	[M/H]	Ref.
6637	1.70	-10.30	9.4	2.1	9.3	1.3	-1.2	0.14	14.87	-0.77	-0.57	VOF05
6638	7.90	-7.15	10.3	2.9	10.2	0.3	-1.8	0.43	15.07	-1.00	-0.78	VOF05
6642	9.81	-6.44	8.6	1.8	8.4	1.5	-1.0	0.60	14.68	-1.20	-0.99	tw
Ter 3	-14.92	9.19	8.1	2.4	7.7	-2.1	1.3	0.73	14.54	-0.82	-0.63	tw
Ter 5	3.81	1.67	5.9	2.1	5.9	0.4	0.2	2.38	13.87	-0.34	-0.14	tw
Ter 6	-1.43	-2.16	6.7	1.3	6.7	-0.2	-0.3	2.35	14.13	-0.62	-0.43	tw

* For these clusters the metallicity estimates ([M/H]) have been derived by using the FVO06 empirical method.

Photometry References: tw - this work

Table 2. Observed and bolometric magnitude of the HB red clump, RGB bump and tip for the global sample of bulge clusters.

Name	[Fe/H]	[M/H]	J^{RC}	H^{RC}	K^{RC}	J^{Bump}	H^{Bump}	K^{Bump}	J^{Tip}	H^{Tip}	K^{Tip}	M_{Bol}^{Bump}	M_{Bol}^{Tip}
6256	-1.63	-1.43	—	—	—	—	—	—	10.63	9.51	9.21	—	-3.56
6266	-0.99	-0.80	—	—	—	13.50	12.75	12.65	9.26	8.10	7.85	0.44	-3.56
6273	-1.40	-1.21	—	—	—	13.65	13.05	12.85	9.67	8.83	8.57	0.10	-3.59
6293	-1.73	-1.55	—	—	—	—	—	—	10.17	9.43	9.24	—	-3.23
6304	-0.75	-0.56	13.55	12.85	12.70	14.03	13.33	13.13	9.06	8.02	7.65	1.10	-3.59
6316	-0.58	-0.38	14.93	14.25	—	15.20	14.65	—	10.28	9.17	—	—	—
6342	-0.71	-0.53	14.25	13.60	13.40	14.65	13.85	13.75	9.71	8.67	8.35	0.98	-3.69
6355	-1.42	-1.22	—	—	—	—	—	—	10.19	9.30	8.92	—	-3.61
6380	-0.87	-0.68	14.95	14.15	13.85	15.15	14.25	13.95	10.37	9.12	8.75	0.62	-3.88
6388	-0.61	-0.42	14.90	14.27	14.17	15.18	14.47	14.33	10.24	9.47	8.81	0.88	-3.76
6401	-1.37	-1.20	—	—	—	—	—	—	10.21	9.07	8.69	—	-3.42
6440	-0.49	-0.40	14.75	13.80	13.60	15.30	14.35	14.13	10.02	8.85	8.33	1.16	-3.82
6441	-0.68	-0.52	15.20	14.55	14.40	15.70	14.85	14.77	10.47	9.49	9.12	1.10	-3.90
6528	-0.17	+0.04	14.15	—	13.35	15.10	—	14.05	9.16	—	7.85	1.74	-4.06
6539	-0.79	-0.60	14.65	13.85	13.65	14.90	14.05	13.83	10.08	8.92	8.47	0.71	-3.77
6553	-0.30	-0.09	13.35	—	12.40	14.05	—	13.05	8.56	—	6.92	1.28	-3.86
6569	-0.85	-0.66	14.95	14.40	14.25	14.93	14.23	14.08	10.52	9.49	9.21	0.55	-3.59
6624	-0.63	-0.48	13.95	13.40	13.25	14.45	13.60	13.65	9.30	8.37	8.08	1.07	-3.85

Table 2—Continued

Name	[Fe/H]	[M/H]	J^{RC}	H^{RC}	K^{RC}	J^{Bump}	H^{Bump}	K^{Bump}	J^{Tip}	H^{Tip}	K^{Tip}	M_{Bol}^{Bump}	M_{Bol}^{Tip}
6638	-1.00	-0.78	14.65	14.05	13.85	14.45	13.73	13.58	9.86	8.89	8.61	0.49	-3.88
6642	-1.20	-0.99	—	—	—	13.85	13.17	—	9.92	8.92	—	—	—
Ter3	-0.82	-0.63	14.27	13.57	13.42	14.37	13.73	13.50	9.95	8.91	8.42	0.54	-3.47
Ter5	-0.34	-0.14	15.15	13.80	13.35	15.75	14.50	13.90	10.25	8.68	7.99	1.32	-3.96
Ter6	-0.62	-0.43	15.10	14.07	13.48	15.75	14.45	14.00	10.56	9.06	8.33	1.01	-3.89

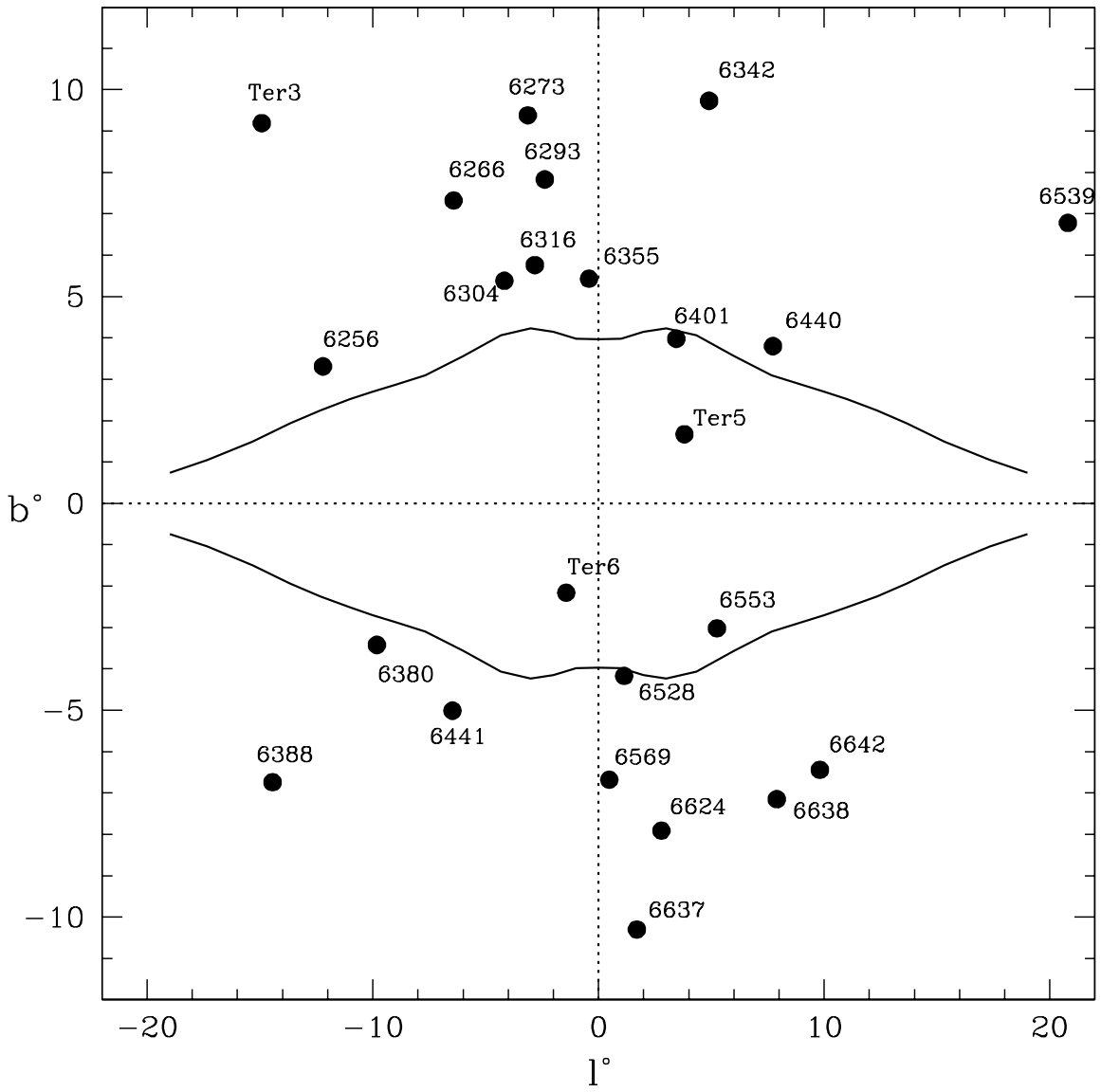

Fig. 1.— Position of the Bulge clusters global sample with respect to the COBE/DIRBE 3.5μm inner Bulge outline (*solid line*, Weiland et al. (1994)) at 5 MJy sr^{-1}.

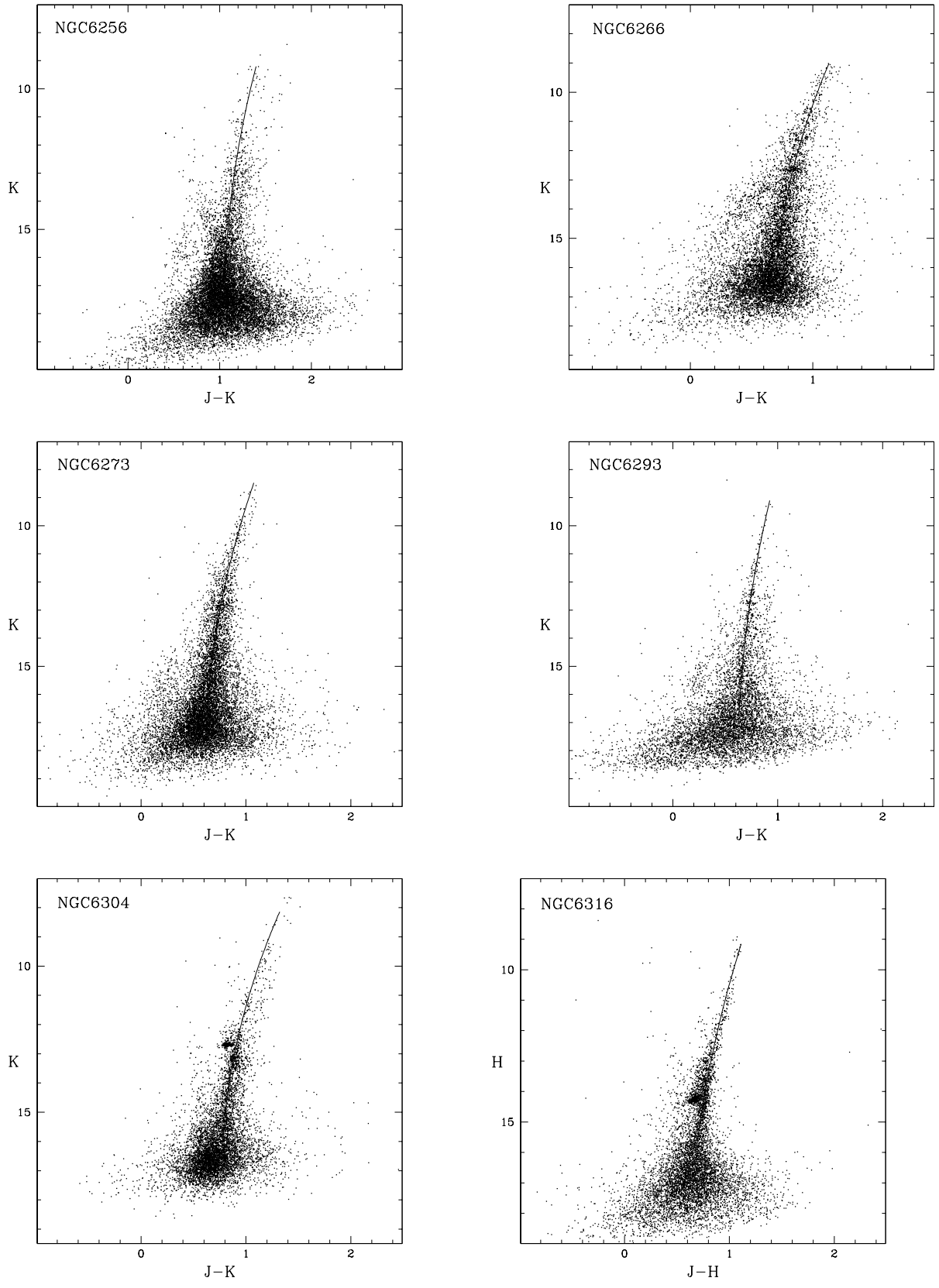

Fig. 2.— Observed near–IR CMDs and derived RGB ridge lines for the global cluster sample.

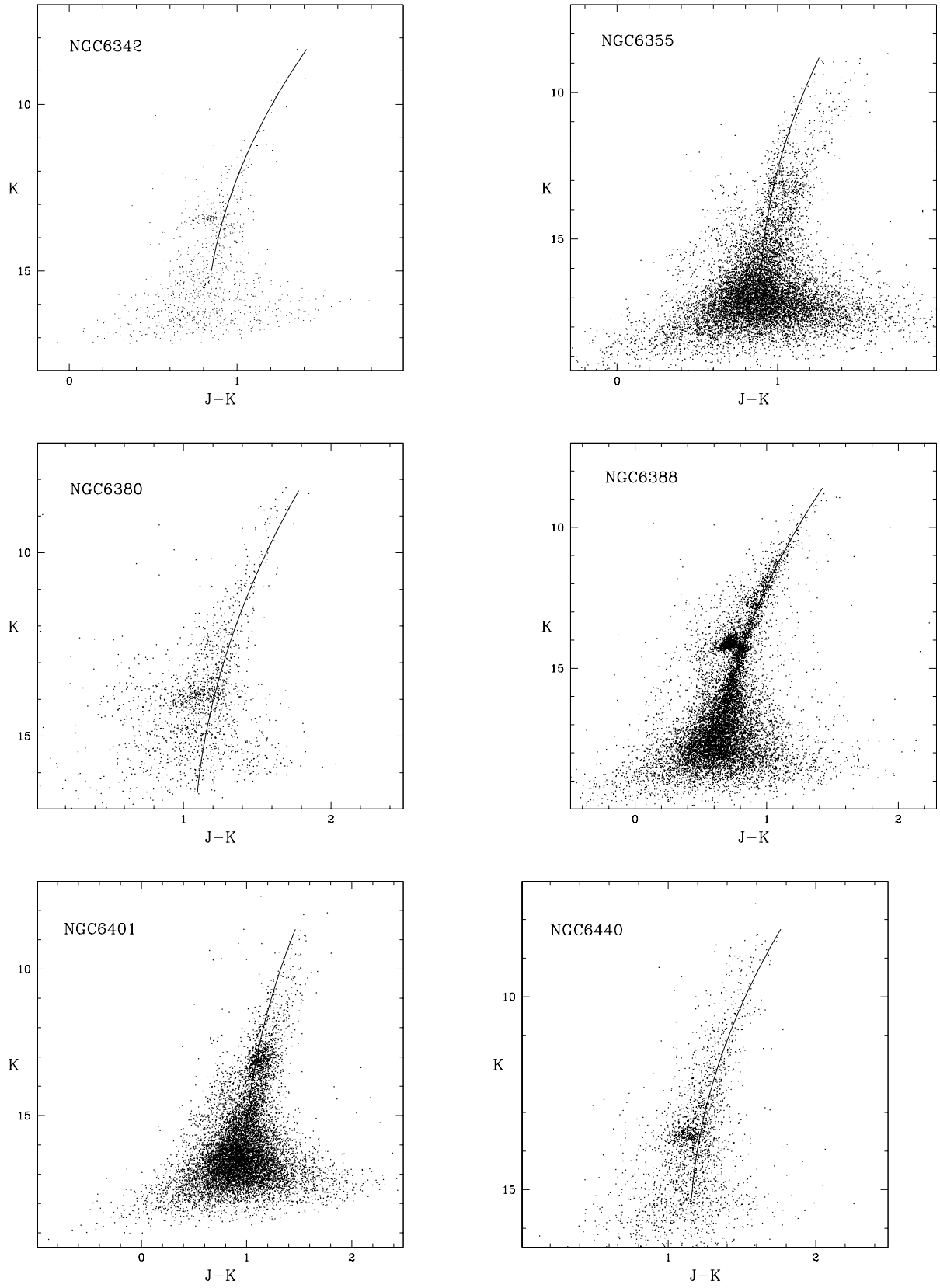

Fig. 2.— continued.

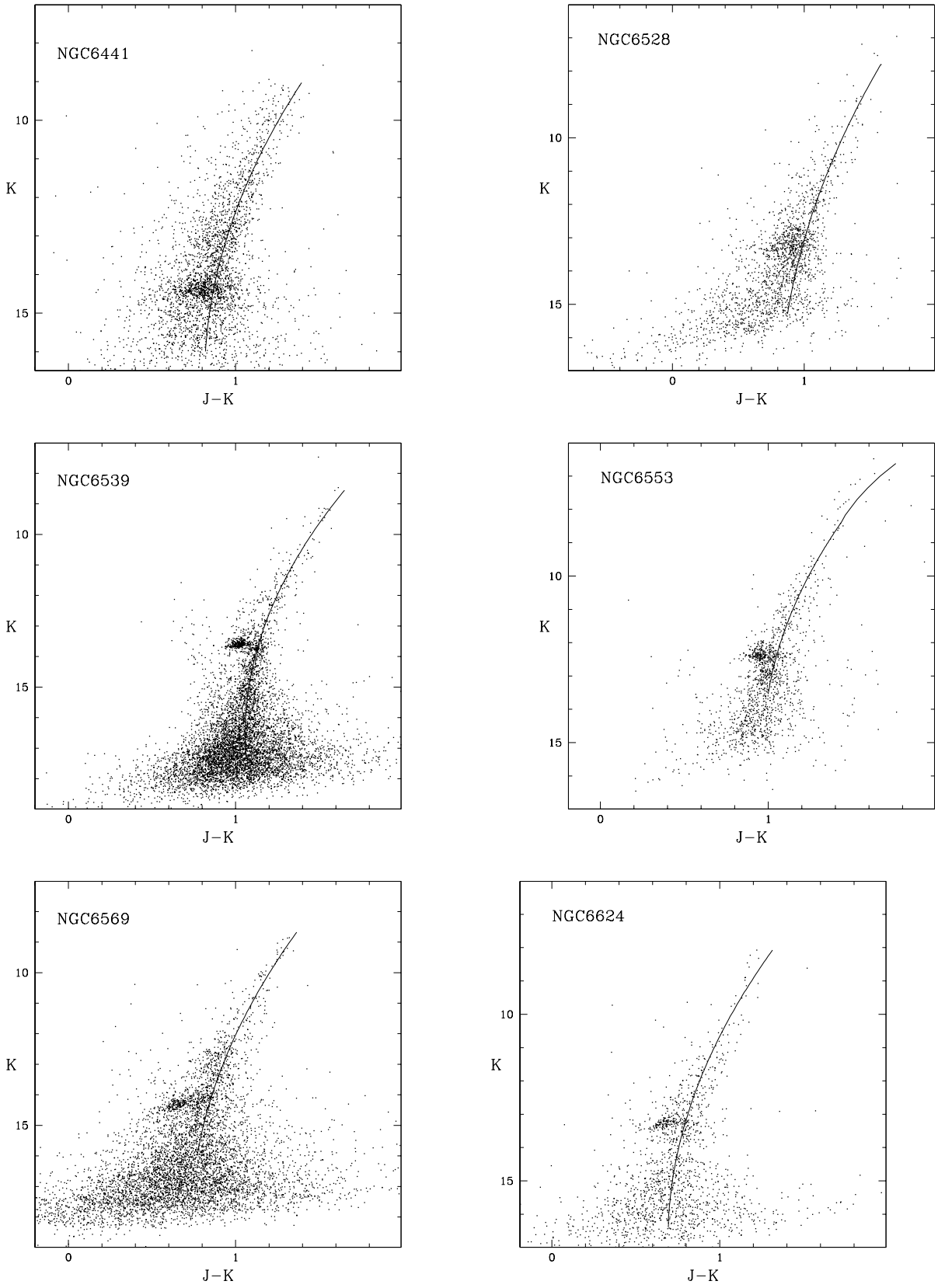

Fig. 2.— continued.

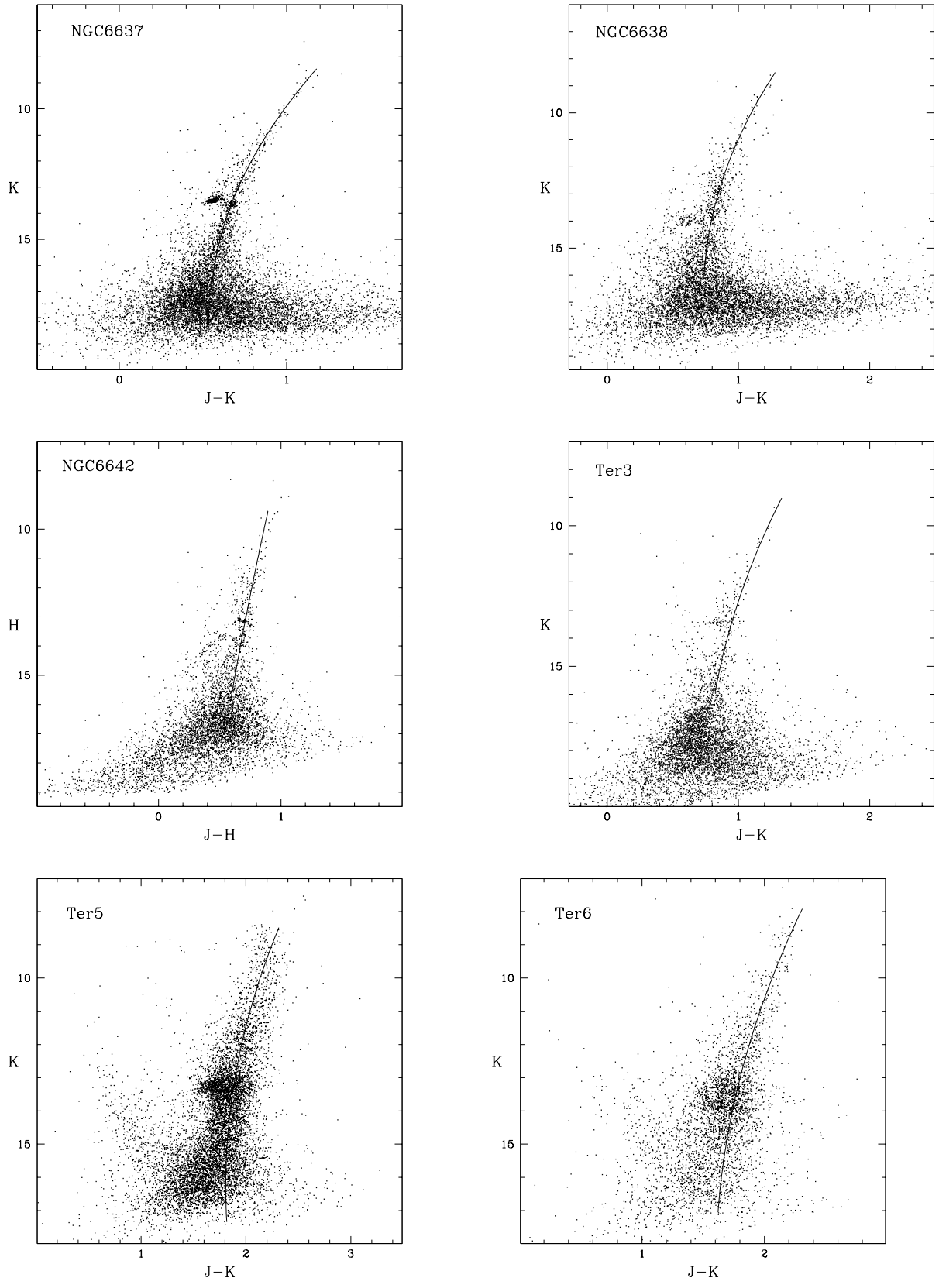

Fig. 2.— continued.

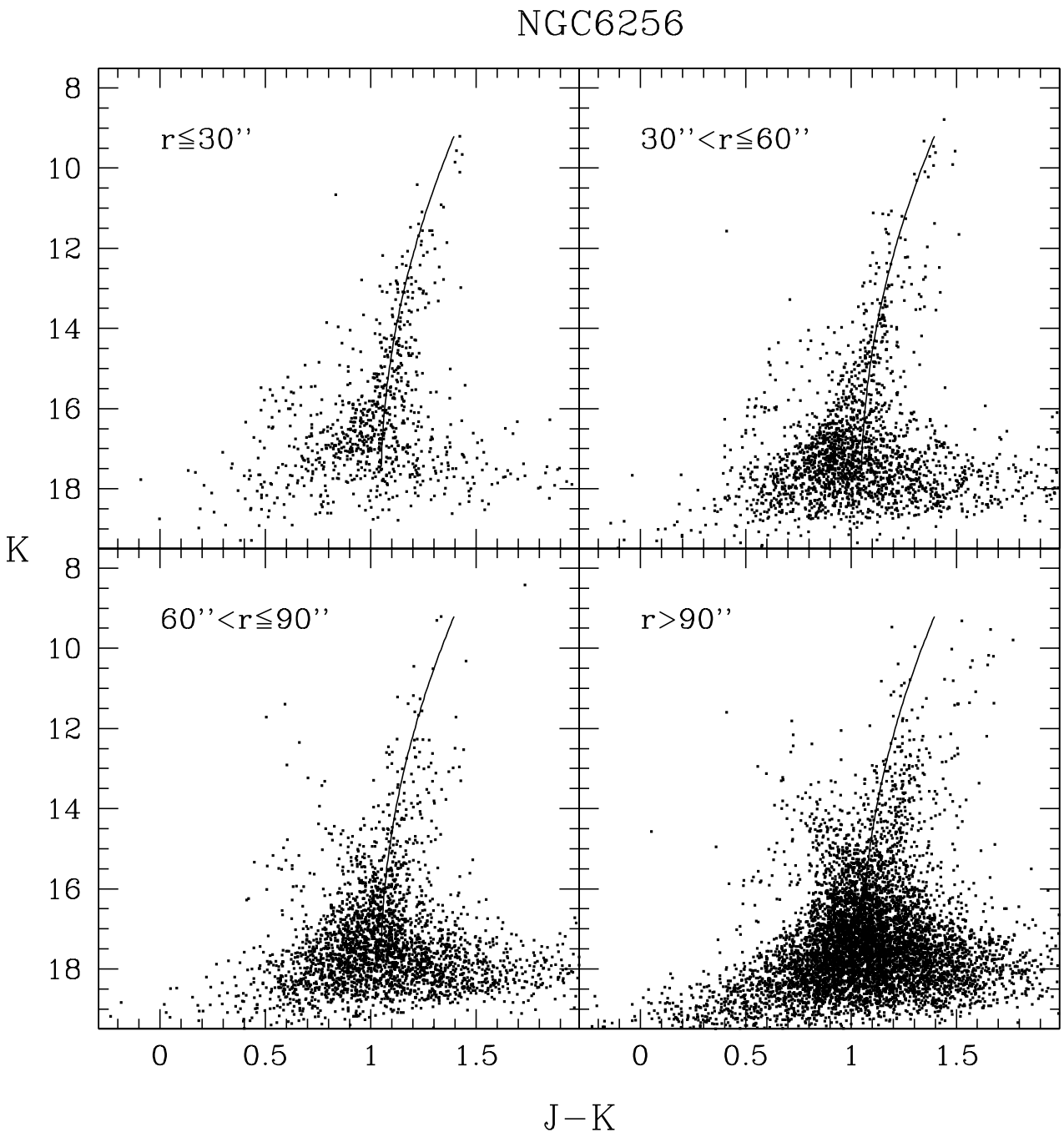

Fig. 3.— [K, J–K] CMDs of NGC 6256 at different distances (r) from the cluster center.

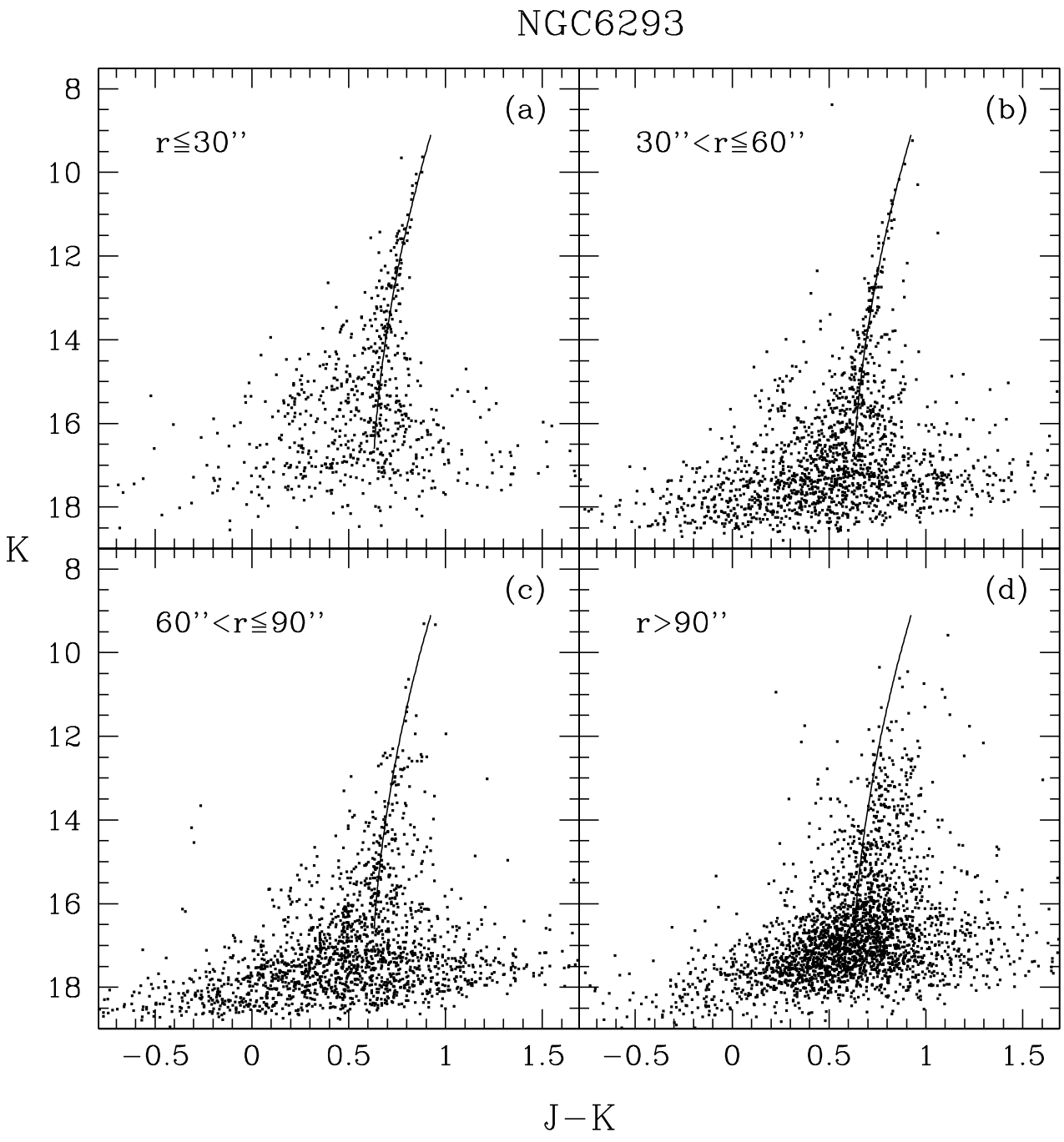

Fig. 4.— [K, J–K] CMDs of NGC 6293 at different distances (r) from the cluster center.

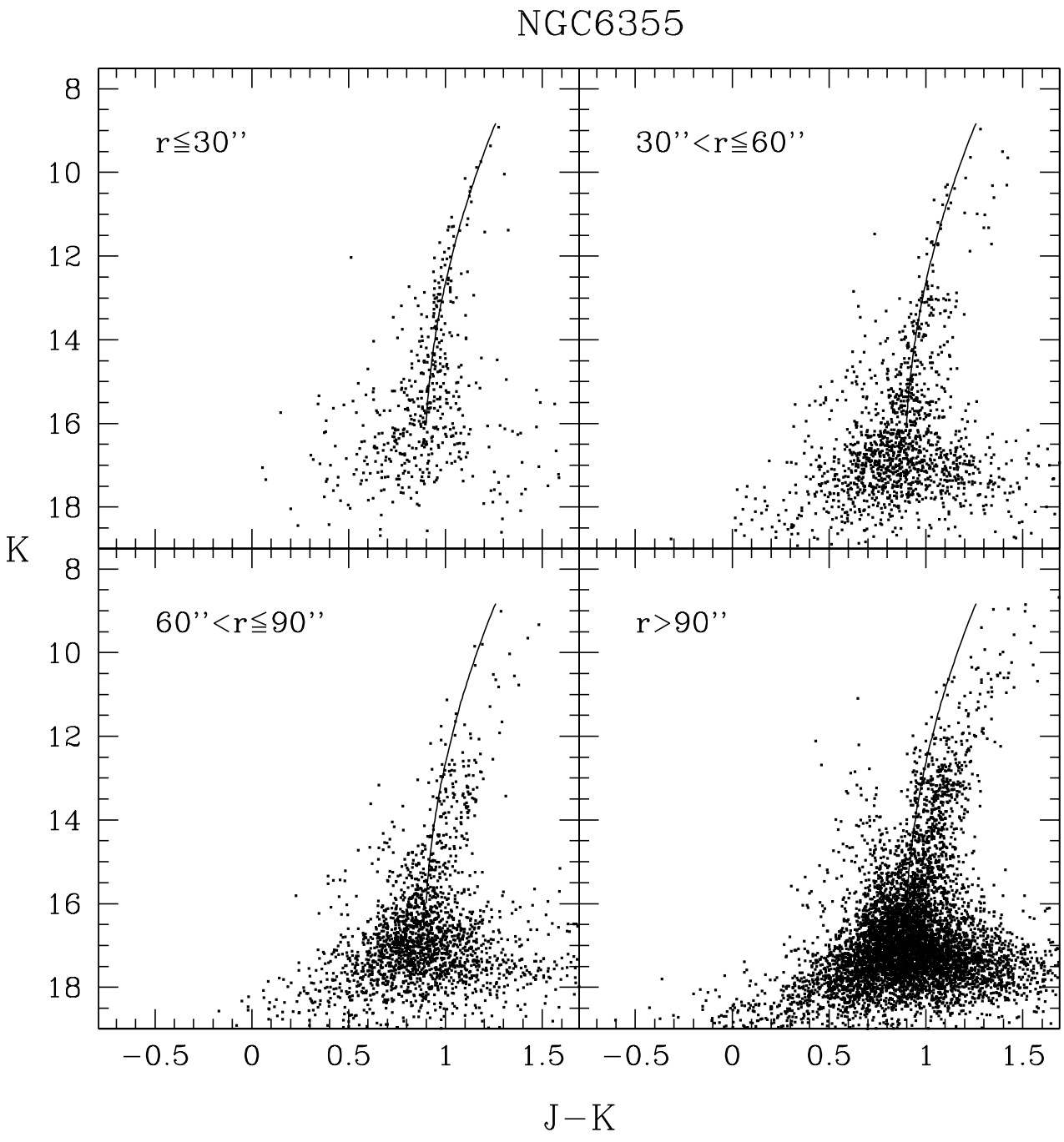

Fig. 5.— [K, J–K] CMDs of NGC 6355 at different distances (r) from the cluster center.

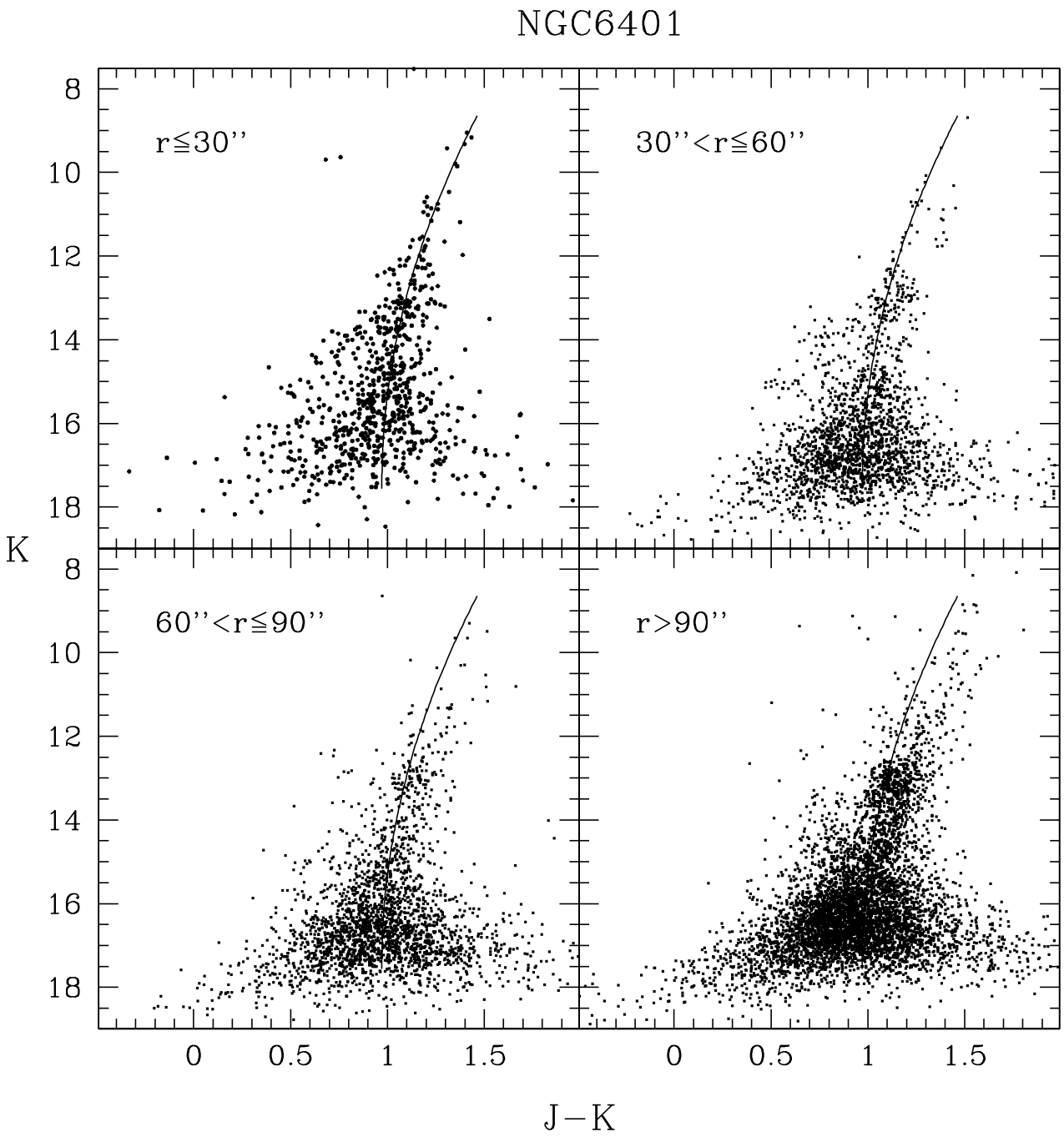

Fig. 6.— [K, J–K] CMDs of NGC 6401 at different distances (r) from the cluster center.

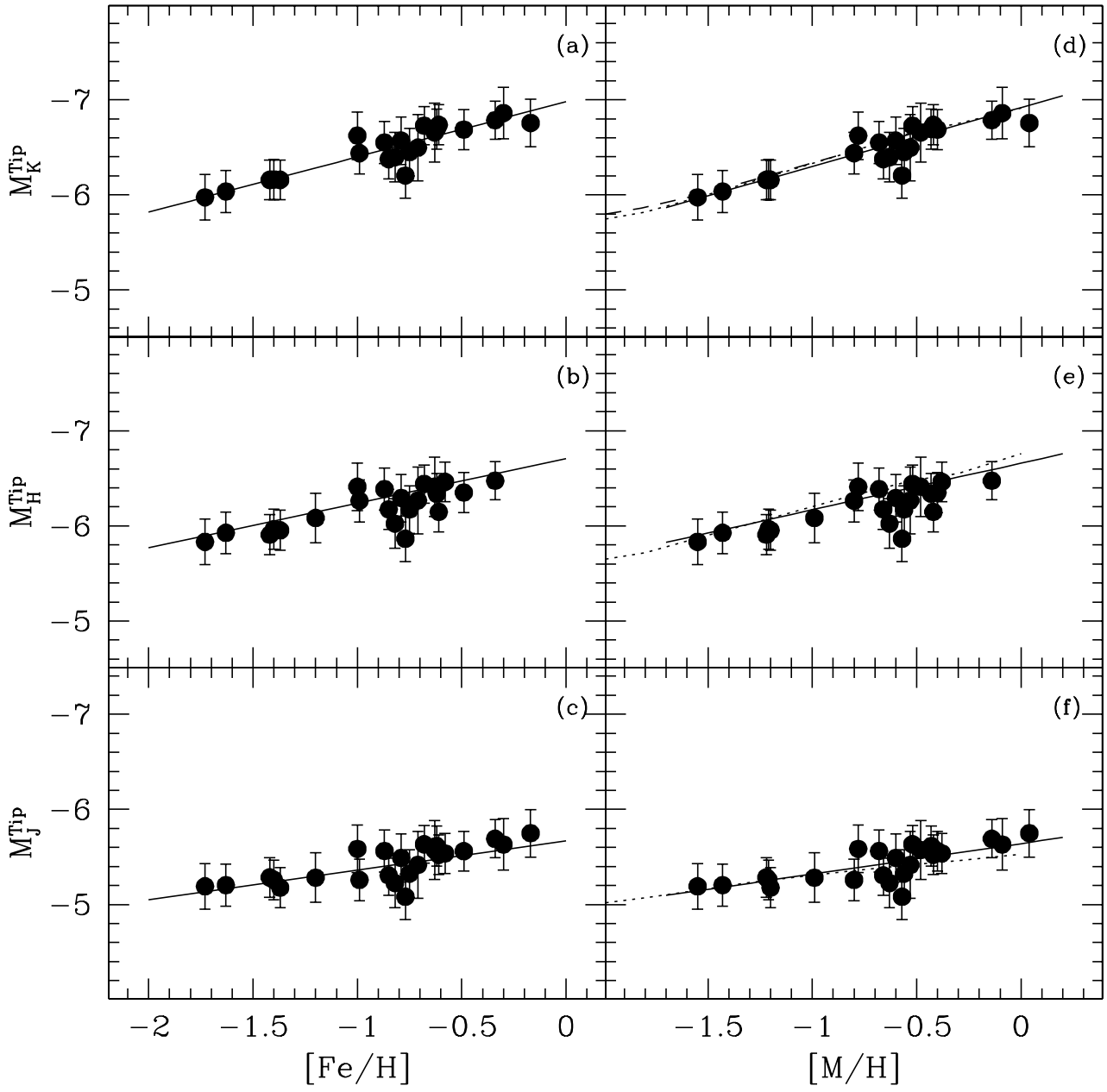

Fig. 7.— The J, H and K absolute magnitudes of the RGB tip as a function of [Fe/H] (panels a, b, c) and [M/H] (panels d, e, f) metallicities for the clusters sample. The solid lines are the empirical relations from VFO04b, the dashed line is the theoretical prediction by Straniero, Chieffi & Limongi (1997), and the dotted lines are the Cassisi et al. (2000) models.

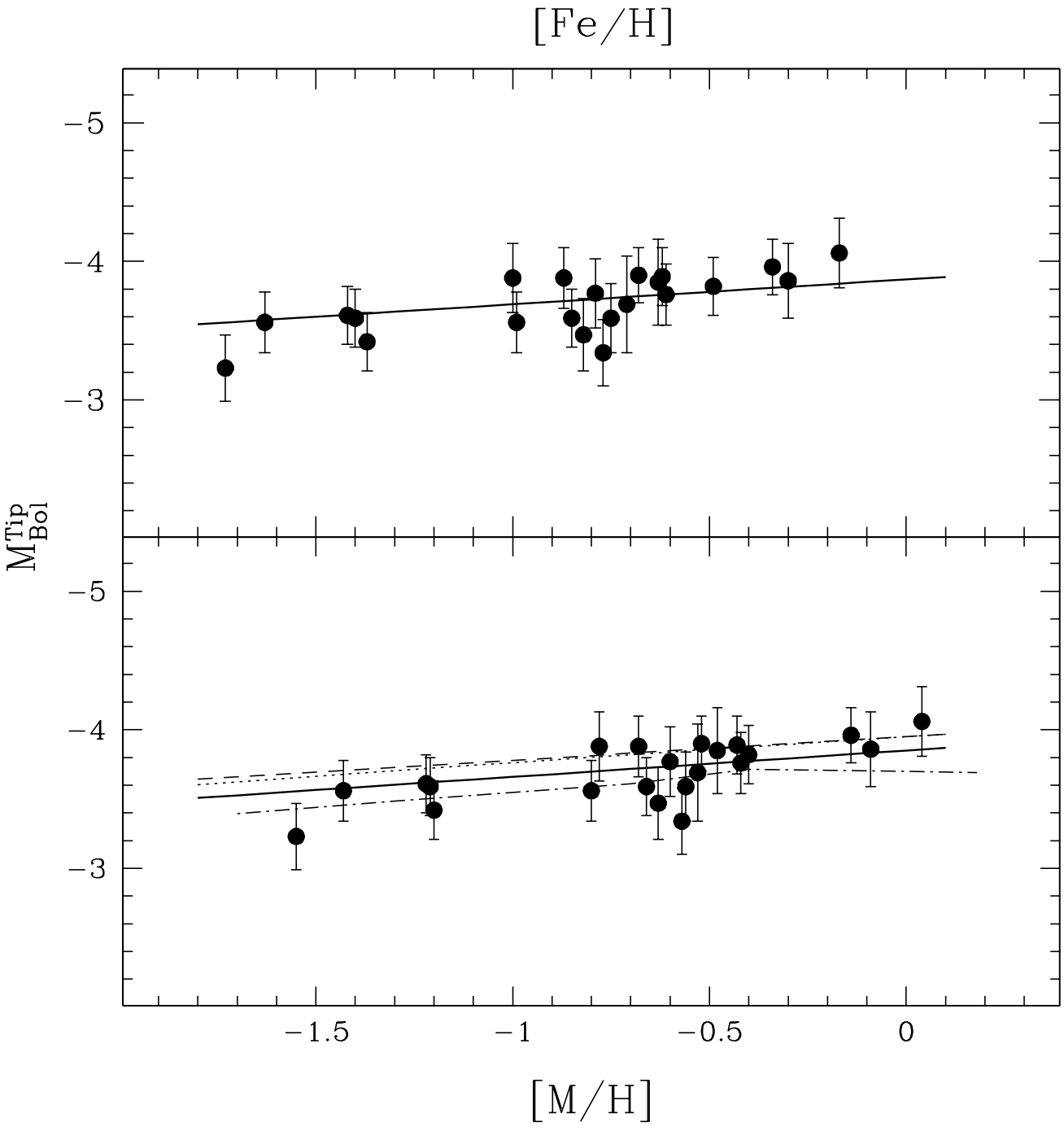

Fig. 8.— Bolometric magnitudes of the RGB Tip as a function of the cluster [Fe/H] (top panel), and [M/H] (bottom panel) metallicities. The solid lines are the empirical relation from VFO04b. Three theoretical predictions have been plotted in the bottom panel: Caloi et al. (1997) (dashed line), Salaris & Cassisi (1997) (dotted line), and Girardi et al. (2000) (dotted–dashed line).

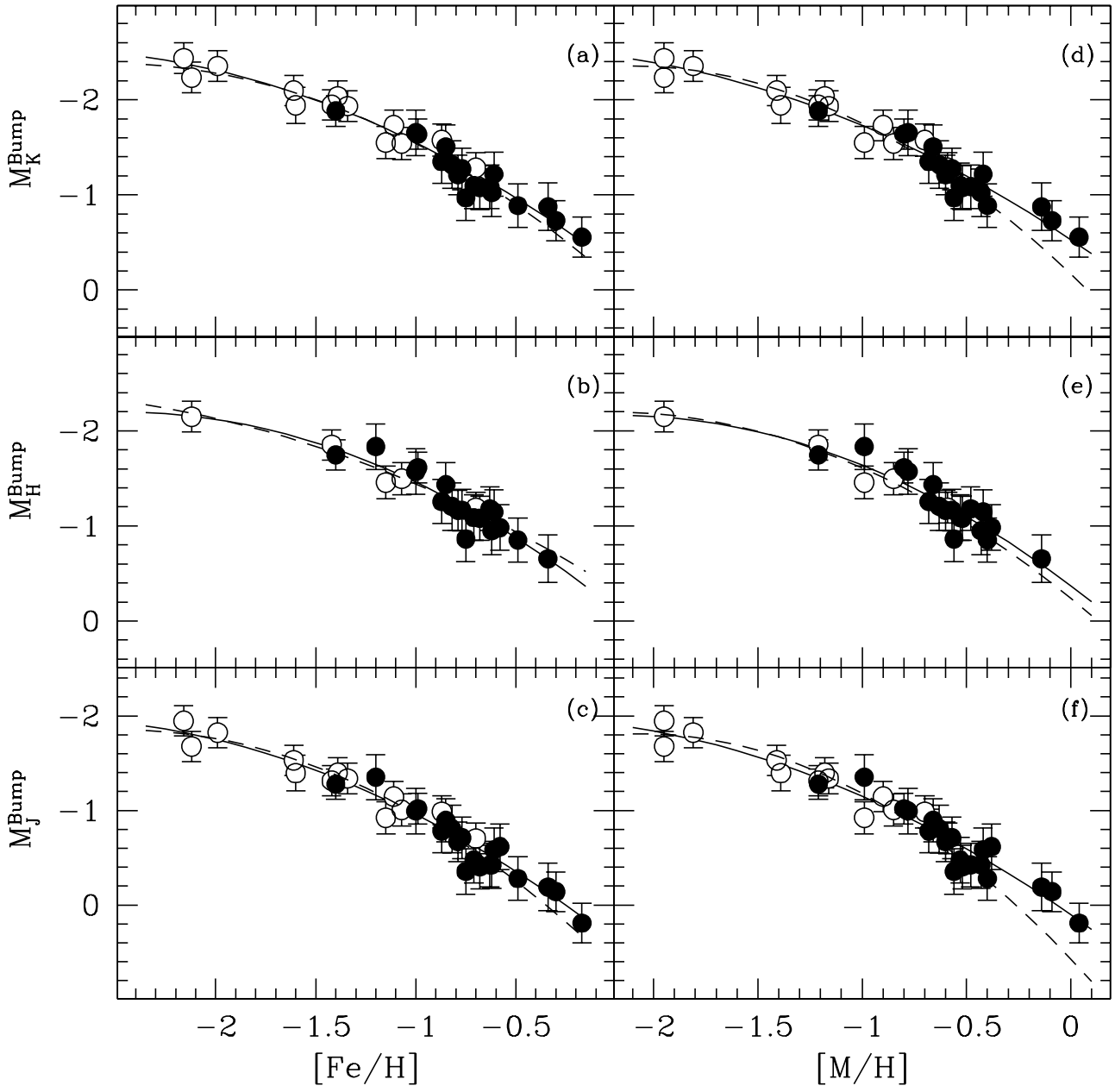

Fig. 9.— The J, H and K absolute magnitudes of the RGB bump as a function of the cluster [Fe/H] (panels a, b, c) and [M/H] (panels d, e, f) metallicities. Filled circles, programme bulge clusters; empty circles, halo clusters presented in VFO04b. The solid lines are the new best-fitting relations. The dashed lines are the VFO04b calibrations.

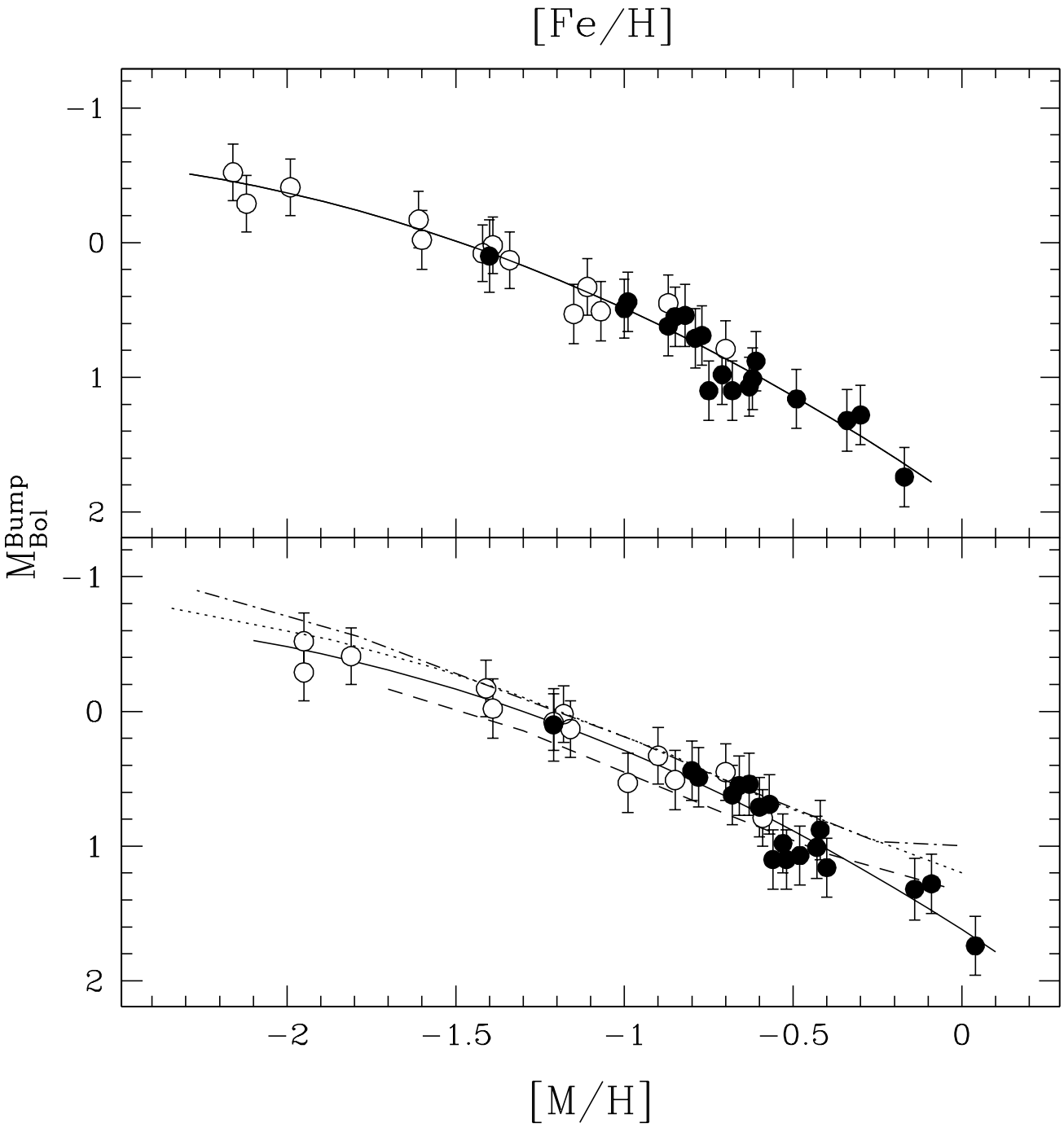

Fig. 10.— Bolometric magnitudes of the RGB Bump as a function of the cluster [Fe/H] (upper panel) and [M/H] (lower panel) metallicities. Filled circles, programme bulge clusters; empty circles, halo clusters presented in VFO04b. The solid lines are our best--fitting relations. Three theoretical predictions have been plotted in the lower panel: Straniero, Chieffi & Limongi (1997) (dotted line), Girardi et al. (2000) (dashed line), and Pietrinferni et al. (2004) (dashed-dotted line).